DEVELOPMENT OF TRANSMISSION ARCHITECTURE FOR RANGE EXTENSION IN ELECTRIC VEHICLES

A Thesis

by

ANSHUMAN SWAIN

Submitted to the Office of Graduate and Professional Studies of
Texas A&M University
in partial fulfillment of the requirements for the degree of

MASTER OF SCIENCE

Chair of Committee,	Swaminathan Gopalswamy
Committee Members,	Hamid Toliyat
	Douglas Allaire
Head of Department,	Andreas A. Polycarpou

December 2020

Major Subject: Mechanical Engineering

ABSTRACT

Most of the current electric vehicles use a single reduction gear set powertrain architecture as their transmission. This is largely due to the fact that the electric motors, unlike engines, produce very high torques at a wide range of lower rotational speeds. Although such architectures allow for smooth power transmissions, there is still potential for improvement in the motor operation efficiency. The proposed powertrain architecture derives its inspiration from the Electronic Continuously Variable Transmissions (E-CVTs) which employ Motor-Generator Units (MGUs) and Planetary Gear Trains (PGTs) to achieve a wide and a continuous range of gear ratios. The E-CVTs have been successful in increasing the fuel economy of Hybrid vehicles and since range anxiety continues to be a prime hurdle in large scale adaptation of electric vehicles, the possibility of using this technology to achieve range extension in electric vehicles is explored.

In this project, a simulation-based approach is used to evaluate a novel E-CVT configuration. The proposed E-CVT has an input-split, output coupled power-path configuration. By modulating the power split ratio between the mechanical (i.e. PGTs) and electrical drivelines (i.e. MGUs), a continuous range of gear ratios that facilitate a higher efficiency motor transmission is obtained. The operation zones for such ratios is subsequently determined through optimization of control strategy with the objective of obtaining a higher end-of-cycle SOC, subject to the vehicular constraints. The performance of the architecture is be bench-marked against both the federal highway and urban driving cycles and a nominal gain of 13.6 percent from the base model range is achieved.

DEDICATION

To my friends, parents and my teachers.

CONTRIBUTORS AND FUNDING SOURCES

Contributors

This work was supported by a thesis committee consisting of Professor Swaminathan Gopalswamy [advisor] and Douglas Allaire of the Department of Mechanical Engineering and Professor Hamid Toliyat of the Department of Electrical and Computer Engineering.

All data obtained for this research has been obtained from sources available through research papers and through open source information sources and have been referenced appropriately.All other work conducted for the thesis was completed by the student independently.

Funding Sources

Graduate study was supported by assistantships from Texas A&M University and from Professor Swaminathan Gopalswamy's CAST LAB.

NOMENCLATURE

PGT	Planetary Gear Train
G1	Basic Gear Ratio of Planetary Gear Train 1
G2	Basic Gear Ratio of Planetary Gear Train 2
MGU	Motor Generator Unit
G'	Transmission Ratio
T	Torque
ω,w	Rotational Velocity
G_{eff}	Effective Transmission Ratio
G_v	Variator Transmission Ratio
a	Acceleration
A_{des},	Desired Acceleration
V_{des}	Desired Velocity
T_r	Regeneration Torque
T_b	Desired Braking Torque
r	Radius of Tire
C0,C1,C2	Friction and Drag Coefficients
I_m	Motor Inertia
I_r	Reflected Inertia
I_w	Wheel Inertia
V_{batt}	Terminal Voltage
SOC	State of Charge
I_{batt}	Cell Current

OCV	Open Circuit Voltage
R_i	Internal Resistance
R_p	Polarisation Resistance
C_p	Polarisation Capacitance

TABLE OF CONTENTS

Page

LIST OF FIGURES

FIGURE Page

LIST OF TABLES

TABLE Page

1. INTRODUCTION AND LITERATURE REVIEW

1.1 Motivation

With the increase in fossil fuel consumption, its detrimental effects on the environment also started to increase and was noticed through global warming caused by a rapid growth in the infusion of greenhouse gases into the atmosphere. It was estimated that transportation contributed 20 percent to 35 percent of the total greenhouse gases. Among the different sectors of transportation, it was also seen that road transport accounts for three quarters of the total energy consumption [1]. Thus, there was a need to develop eco-friendly powertrain for greater sustainability and reduction in the environmental pollution. The automotive industry has tried to answer it by switching to cleaner fuels such as natural gas and bio diesel and also through electric powered vehicles. These changes pertain to the modification of the power source. But there is also another stream of research that has been working to maximize the efficiency of power delivered from the sources to the vehicle. This is where the field of alternative powertrain architectures has gained prominence over the last few years. This literature review is intended to study the new improvements in these architectures and analyze the potential for further increase in application in modern day vehicles. Some of the architectures that will be considered are IVT, (Infinitely Variable Transmissions) for Internal Combustion Engine driven vehicles, Electronic Continuously Variable Transmissions (E-CVT) for hybrid and electric vehicles and some modern approaches in battery and fuel cell driven vehicles.

1.2 Existing Powertrain Architectures

In this section, the various existing architectures that are in use or have been used in IC engine powered vehicles, Hybrid Vehicles and BEV vehicles, for the purpose of improving fuel economy, are mentioned. In IC engines, various architectures with different implementations of the IVT concept are discussed. Similarly, in hybrid vehicles segment, the various ECVT based architectures are explored. Finally, the various new architectures used in Battery electric vehicles are also

mentioned.

1.2.1 Architectures for Internal Combustion Engine run vehicles

Infinitely variable transmissions are those transmissions which use various mechanical coupling devices to provide an infinite gear ratios. Generally these include the Continuously Variable Transmission (CVT), the Planetary Gear Train (PGT) and in some cases, the fixed ratio gearbox.

In the research article by Mantriota (2001) [2], he considered a combination of all the aforementioned components and attempted to determine the operational features of an IVT by regulating the CVT power flow. He studied the effects of using helical springs to produce the requisite axial thrust on both the pulleys to achieve the automatic regulation characteristics. He hypothesized a clock wise power flow between the components and found that the transmission ratio increased with the growth of the input torque. Through anti-clockwise power flow, he determined that the transmission ratio saturated with a limiting value for the applied torque. The system also resulted in efficiency gains due to lack of power actuation as compared to a typical CVT.

Mantriota, along with fellow researchers Carbone and Mangiarlardi (2001) [3], also studied the effects of an IVT on the fuel consumption of a mid-class Vehicle. They implemented a simulation based approach where they optimized the IVT's transmission ratio with the objective to minimize fuel consumption. They considered 3 different drive schedules to validate the performance over varying conditions. In the first case, the fuel consumption rates were compared at constant speeds and subsequently they were measured against the EUDC and ECE-15 drive cycles. The model was further benchmarked against vehicles using manual and CVT transmissions and found that the proposed IVT architecture with series TYPE-1 flow had lower fuel consumption than the CVT and manual gear trains during the constant vehicle speed cycle and this performance superiority was further accentuated at higher speed values. Although the IVT was surpassed by the Robotized Gearbox in the ECE-15 and the EUDC drive cycles, the researchers concluded that with IVT can be considered as an alternative to the regular discretized transmissions in the mid class category due to the exhibition of higher comfort and fuel efficiency.

Bemporad, Mannelli and Borodani (2003) [4], further studied the applications of the motorized

gearbox and supervised its performance using hybrid modeling and control techniques. A motorized gearbox is basically a manual gearbox but has electronically actuated servo motors that provide smoother gear shifting operations than the human driver. The researchers used an MPC (model Predictive controller) to control the gear selection and engine torque response based upon the inputs from the driver. Through optimization, they were able to hypothesize that through proper selection of weights in the MPC, a decrease in the consumption rate as well as emissions was possible through the motorized gearbox thereby establishing it as another alternative powertrain worthy of consideration.

Another variation of the IVT known as GIVT (Geared Infinitely Variable Transmission) was considered by Zhu and Wang (2014) [5]. The GIVT implemented a crank slider mechanism to achieve the designed transmission ratios. The mechanism used planetary gear sets to modify the crank length through a Rack and pinion arrangement resulting in variation in the transmission ratio. To avoid instantaneous changes in the dynamic load, the researchers also introduced non circular gears between the input and the output of the model. The model was then simulated using the MATLAB-SIMULINK environment to obtain the desired ear ratios at the requisite vehicle speeds.

Recently, Culebro and Villar (2019) [6], made recent developments to the field of research in IVT by proposing a design consisting of orbital pulleys. The proposed design consists of two systems. The first system contained a planetary gear connected to a flywheel. The second system consisted of a CVT that altered the transmission ratio. This ratio change was facilitated by opposite movements of both the orbital pulleys maintaining the constant length of the belt. Through experimentation and validation tests, they were able to establish constant output speeds against variations in the input speed thereby allowing smooth changes in the transmission and eliminated the requirement of clutches as it provided a continuous range of gear ratios.

1.2.2 Architectures for Hybrid Vehicles

The ECVT was designed for hybrid vehicles in order to leverage the regenerative capacity of motor-generator units to store energy in the battery. The ECVT is designed to function similar to IVTs but instead of using a CVT, it uses motor generator units to alter the gearing ratios of

planetary gear sets thereby changing the effective transmission ratio of the system. Although this system was primarily developed for hybrid vehicles, it has slowly become a topic of interest for implementation in electric vehicles too.

Miller (2006) [7], researched upon other type of ECVT power splits that were in use in the automotive industry. The first architecture that was used for ECVT was developed by Toyota and was called the Toyota Hybrid system. This system was basically an input split mechanism where the planetary gear train would split the input power from the IC engine into mechanical and electrical power. The mechanical power was routed through output mechanical gearing whereas the electrical path was routed through motors. The next architecture which was considered was that of a compound split architecture that contained a power split device both on the input and output side. It allowed the functioning of the ECVT in two modes. The first mode replicated the architecture of the input split mechanism, whereas in the second mode, both the input and output power split devices functioned as differentials. This type of architecture has been used by General Motors and Allison. Miller concluded the paper with his analysis of the series parallel switching architecture. This contained a single motor that connected the engine to the planetary gear set. This architecture was generally used in rear wheel drive vehicles. The power flow management was easier than other architectures due to presence of lesser torque sources. Also, the architecture facilitated a wide range of motor-generator power levels and could function as a power assist or as a dual mode hybrid.

Sheu (2006) [8], developed another E-CVT but with one motor and two PGTs. A 1-DOF (Degrees of Freedom) PGT is connected with a 2-DOF PGT to facilitate power splitting and combined the power of the Electric motor and the IC engine. It allowed a 5 mode operation to optimize power flows for higher system efficiency. The system had inexpensive implementation and had a simpler structure than the CVT architecture and was proposed to be used in hybrid scooters.

Building upon the research on the use of dual planetary gear sets in the vehicles, Zhang, Peng, Sun and Li (2014) [9], studied another design consisting of multiple PGTs but with the inclusion of clutches. This inclusion of clutches allowed multiple modes of operation. They applied automated

modelling and used an exhaustive approach to model up to 16 clutches and consequently derived 14 different classes consisting of 109 unique feasible driving modes. The infeasible and redundant modes were neglected. The modes were then subjected to the near optimal energy management strategy (PEARS) and the efficient modes were identified.

Ju, Zhuang, Wang, Jiang (2018) [10], hypothesized a new four-wheel drive hybrid electric sport utility vehicle by utilizing the double planetary gears concept. In this concept, they connected the rear axle with an extra motor and implemented the power split architecture. They also applied discrete dynamic programming to calculate the optimal control strategy to achieve the best fuel economy. The concept was benchmarked using the Federal urban driving schedule (FUDS) and the Highway fuel economy test schedule (HWFET). It was found that the fuel economy increased by 41.4 percent the FUDS cycle and 19.5 percent under the HWFET cycle when compared against a typical gasoline engine driven vehicle.

In the research paper published by Chung, Wu and Hung (2018) [11], they classified the ECVTs into three categories namely upward circulation, downward circulation and neutral circulation, based upon the ratio of circulating power of the system. The analyzed the two power split systems (input split and output split) and recorded their effects on the vehicle efficiency. It was found that the input split displayed characteristics of the downward circulation suitable for driving at low speed at high driving loads, whereas the output split had characteristics of the upward circulation and favored high speed driving at lower loads. They compared the planetary gear set and dual clutch powertrain developed by Chung et al. (2000) [12], with the Toyota hybrid system and derived the optimal points of operation for maximizing fuel efficiency. They recommended the development of an architecture that allows for both upward and downward circulation modes and facilitates switching between the two upon change of load and speed.

1.2.3 Architecture for Battery Electric Vehicles

Although electric vehicles are more suited to the implementation of an E-CVT transmission, Bottiglione, Pinto, Mantriota and Sorniotti (2014) [13], hypothesized an IVT implementation for electric vehicles. They considered an architecture where an IVT was connected to the electric mo-

tor as the power source and channelized the power to the vehicle wheels. Their simulation based approach studied the previously mentioned series and parallel IVT configurations and compared the energy consumption of the battery against those equipped with single speed, two-speed and CVT transmissions. It was found that the IVT architecture had higher efficiencies than the traditional single speed reduction gearbox, currently in use in the electric vehicle sector, over the urban driving cycle.

Another possibility of improvement in the range extension of Electric vehicles comes from the application of multi speed gearbox transmissions. Although this is not a novel concept, it grants a good insight into the optimization of operating modes including the high torque producing electric motors. Ruan, Walker, Wu and Zhang (2017) [14], published a paper regarding the development of a CVT based and a multi-speed dual-clutch based transmission designs for the electric vehicle. The dual clutch model consisted of having two sets of parallel shafts connected with a common clutch. In a two-speed DCT, synchronizer use is avoided and shifting is facilitated through fixed ratio clutches. I was found that due to addition of complexities in gear shifting and the overall weight of the vehicle, the multi speed gearboxes exhibited lower transmission efficiency than the single speed gearbox, but due to modification in the shifting strategy, the multi speed gearboxes achieved higher energy utilization efficiency. Similarly , it was noticed that the CVT produces significant gains over the multi-speed transmission during the regenerative phase as in multi-speed, shifting to a lower gear is actuated leading to torque interruptions which consequently results in less charging of the battery.

Lastly, In-wheel motor systems are also gaining popularity in the small electric vehicle section. Kim, D., Shin, Kim, Y. and Cheon [15], studied the integration capability of such systems in the rear section of cars. They considered a system containing a PGT as a gear reducer connected directly with the motor. It was found that the PGT size was one of the major components that not only impacted the overall packaging but also affected the vehicle mass and suspension parameters. Due to the independence in motor operations, such drivetrains could replace E-CVTs in the EV market in the future.

Thus, through this review we were able to gauge the rapid development and the growing research impetus on alternative drive train architectures. Most of these concepts have been inclined toward maximizing fuel and energy efficiency, whereas some of the other designs have prioritized the ease and simplicity of operations. In the IC engine field, IVTs have been the most dominant form of the alternative powertrain by providing superior fuel economy. In the Hybrid segment, E-CVTs have emerged as the major technology due to its regenerative capacity. Whereas in the Battery driven sector, single reduction gearbox transmissions are the norm but ECVTs have the potential to be the choice of architecture for the OEMs in the future and are thus required to be studied. In subsequent chapters, through system level analysis, simulation and optimization, a transmission architecture is developed with the purpose of achieving a substantial increase in the nominal Range of Electric Vehicles and the performance is bench-marked against an existing low weight passenger car.

2. IDEA CONCEPTION AND BACKGROUND

2.1 Main Idea

For any automotive vehicle, the conversion of stored chemical energy into usable mechanical power is characterized using a basic system flow as shown in fig(2.1).

Figure 2.1: Power train flow chart in vehicles.

The power source generally consists of two components, an energy source which provides the requisite chemical energy (e.g. Batteries for Electric Vehicles and Fuel tank for IC engine powered vehicles) and a prime mover that converts the chemical energy into mechanical power (Motors for EVs and IC engine for fuel powered vehicles). Electric batteries have lower energy densities than hydrocarbon fuel but the conversion efficiency through motors is higher than that of an IC engine (around 40 percent).

The transmission refers to the application of mechanical transmission devices such as single-reduction gearbox, planetary gear trains (PGTs) and Continuously Variable Transmissions (CVTs), for the transmission of the power from the power source to the vehicle.

The Vehicle refers to the performance parameters of the mobile body characterized by the harvesting of the transmitted mechanical power into motion. This is modeled through vehicle

dynamics equations and the vehicle velocity and acceleration are calculated accordingly.

2.2 Range Improvement Strategies

Using the aforementioned power flow design, some of the methods through which an increase in the nominal range of vehicles could be achieved are listed below-

- Increase energy content at source : This is a trivial solution which envisages having higher energy availability at the source for our disposal, inevitably leading to an increase in the nominal range. In the field of pure electric vehicles, this approach has seen a growing amount of research as battery energy density still has scope for further development and is being heavily investigated by all the major OEMS (Original Equipment Manufacturer) in the electric market.

- Improve transmission efficiency : Another method of Improving the range would be to improve the efficiency at which the harvested power is transmitted to the vehicle. This relates to the efficiency of mechanical transmissions, which in the case of EVs are the single set reduction gearbox and the PGTs which have already achieved a high operational efficiency of 95 percent. Thus scope for improvement in this field is relatively lower.

- Improve efficiency at the source : This includes improving the efficiency at which the energy at the source is harvested as mechanical power by manipulating the operation points of the prime mover through optimization. Such approaches have been implemented in hybrid transmissions in the form of IVTs (Infinitely Variable Transmissions) and E-CVTs (Electric Continuously Variable Transmission) and have resulted in an increase in the fuel economy.

In this thesis, the third method is investigated for its potential for applicability in electric vehicles. The trade off is between the efficiency gained by operating the prime mover in its optimal island and the efficiency lost through transmission of power using motors and mechanical gearboxes used to facilitate a continuously variable transmission architecture. The Toyota Prius (2003) transmission system is considered for initial analysis and the architecture is developed based upon the results of the analysis.

Expanding on the idea further, the power split flow in the given architecture during cruise conditions is shown in fig (2.2)

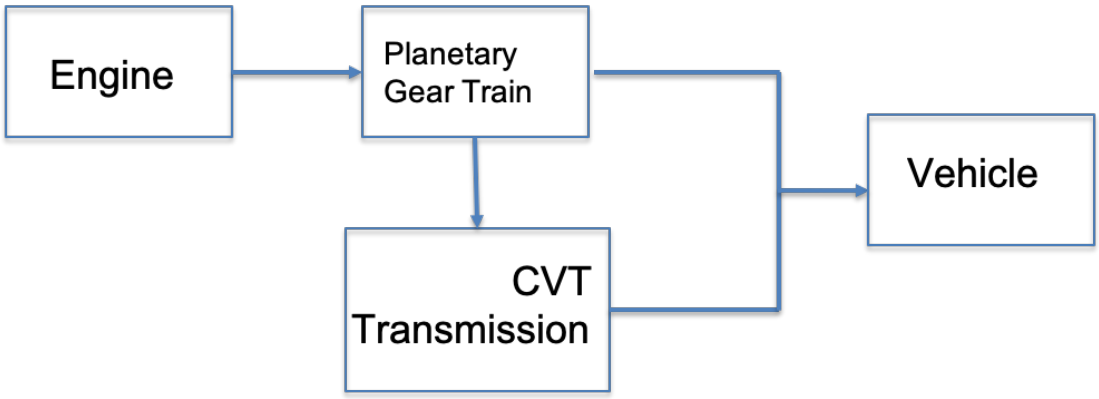

Figure 2.2: A Typical E-CVT Architecture in Hybrid Vehicles.

The implementation of the CVT transmission allows the engine to operate at high efficiency operation island as long as possible while delivering the requisite power at the wheel. Now nominal efficiencies of PGTs are around 95 percent - 97 percent whereas for CVTs or ECVTs it varies from 80 percent - 90 percent. Thus to achieve maximum range , the architecture should be operated for a wide continuous range of transmission ratios with minimal power flow through the variator.

2.3 Toyota Prius (THS-II) Architecture

The Toyota Hybrid System, also known as the Hybrid Synergy Drive (HSD) was upgraded by Toyota in 2003 to be used in its hybrid class of vehicles. The system uses an architecture which utilizes motors and PGTs to achieve a continuously variable transmission configuration also known as E-CVT.

The Hybrid Synergy Drive architecture used in the Toyota Prius is shown below in fig(2.3)[16].

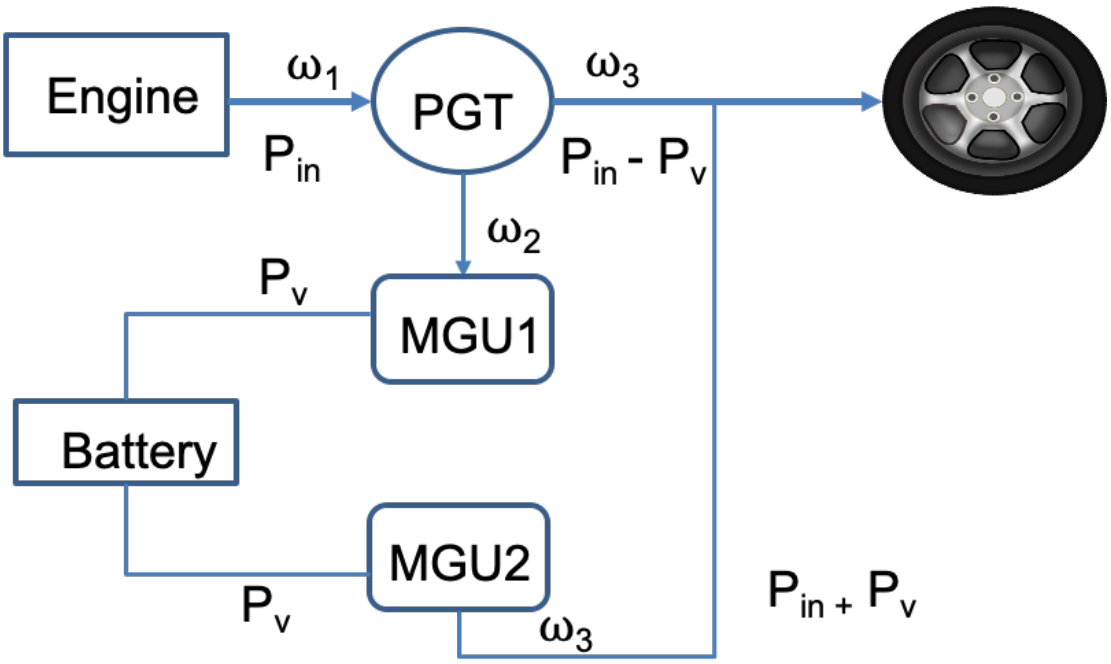

Figure 2.3: Hybrid Synergy Drive Architecture Used in Toyota Prius.

This architecture is run through an implementation of a computer driven control strategy that is dependent upon the current operating condition of the vehicle. At low speeds or at start, only the electric motors are used due to their higher performance efficiency when compared to the ICE. In the cruising and the acceleration phase, the engine power is split between the electro-mechanical components. One part of the engine power is used directly to run the vehicle. The other part of the engine power is used to operate MGU1 as a generator to harvest the electrical energy and charge the battery in case of a low SOC (State of Charge). If the SOC is not low, then the harvested energy is used to run MGU2 to supplement the requirements of the driver. In cases of extreme acceleration, the entirety of the engine power is delivered to the wheel and is compounded by addition of more power through MGU2. During the braking phase of the vehicle, the vehicle's kinetic energy is used to run both the MGUs in generator mode in order to increase the SOC of the battery.

This type of a power split architecture , as mentioned before, has potential for implementation in electric vehicles although with some necessary considerations. Unlike hybrid vehicles, Battery

Electric Vehicles (BEVs) function only with motors as the source of power. Thus unlike in hybrid vehicles, if the battery SOC becomes zero, the motors cannot be run and thus the battery cannot be recharged. Therefore, for our analysis, we will only consider the operation ability of this architecture in the cruise phase.

2.4 Kinematic Analysis of Planetary Gear Sets

In this section, some of the associated kinematic relationships which are intrinsic to the function of the planetary gear sets are discussed. This is done to facilitate a better understanding of the functionality and working of PGTs and these fundamental equations are also used in subsequent sections for control strategy and parameter modelling.

Planetary Gear Trains are a form of mechanical gear sets which possess two degrees of freedom (DOF). They are generally used in compound sets of transmission to provide multiple gear ratios. They also act as power split and power compounding devices in various infinitely variable configuration set ups . PGTs consist of a sun gear, a planetary carrier connecting all the planet gears and the ring gear in the outermost periphery. As a consequence of being a 2 - DOF system, speeds of any 2 components automatically constrains the speed of the third component.

If multiple planetary gear sets are connected in such a way where they exhibit two degrees of freedom, then the relationship between the multiple branches of the planetary gear sets are characterised by the transmission ratio

Transmission Ratio (G'): The ratio between the relative speed of input gear with respect to controlled gear to that of the relative speed of the output gear with respect to controlled gear.

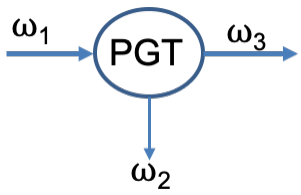

Figure 2.4: Schematic Representation of Speeds in a PGT System.

In fig(2.4), The PGT represents a 2 DOF set of multiple interconnected PGTs, $\omega 1$, $\omega 2$ and $\omega 3$ represent the input speed, the controlled speed and the output speed of the PGT set respectively. The functional form of G'is shown in equation (2.1).

$$G' = \frac{\omega 1 - \omega 2}{\omega 3 - \omega 2} \tag{2.1}$$

This is applicable in a broader sense to all planetary gear set combinations with 2 DOF. In the case of a single planetary gear train, the speeds of the sun, ring and planetary carrier are characterized by Basic ratio of a PGT.

Basic ratio (G): The ratio between the relative speed of the sun gear with respect to the planetary carrier to that of the relative speed of the ring gear to the planetary carrier.

The functional form of the Basic ratio is shown in equation(2.2). ω_s, ω_c and ω_r represent the speed of the sun gear, planetary carrier and the ring gear of a single PGT respectively. R_r and R_s represent the radius of the ring gear and sun gear respectively.

$$G = \frac{\omega_s - \omega_c}{\omega_r - \omega_c} = \frac{-R_r}{R_s} \tag{2.2}$$

Both G' and G can be represented in terms of each other. In our analysis , we have used G as the characteristic feature for single planetary gear set systems in this report.

In an Inertia free and friction less assessment, the net torque and the net power transmitted through the PGT is conserved. in subsequent equations, T represents the Torques in the respective branches of the PGT [7].

$$T_s + T_r + T_c = 0 \tag{2.3}$$

$$T_s * \omega_s + T_r * \omega_r + T_c * \omega_c = 0 \tag{2.4}$$

By solving equation (2.2), equation(2.3), equation(2.4), the following relationships between

the torques of the branches of a planetary gear train is achieved,

$$\frac{T_s}{1} = \frac{T_r}{-G} = \frac{T_c}{G-1} \tag{2.5}$$

Some other nomenclature which are used in this report and are required for the analysis of the architecture are mentioned subsequently.

Effective transmission ratio (G_{eff}): Ratio between the input and output rotational speed of the transmission system. In fig (2.3), the effective transmission is given by the following formulation-

$$G_{eff} = \frac{\omega_1}{\omega_3} \tag{2.6}$$

Variator transmission ratio (G_v): Ratio between the input and output rotational speed of the variator (MGU1 + MGU2)transmission system. In fig (2.3), the variator transmission is given by the following formulation-

$$G_v = \frac{\omega_2}{\omega_3} \tag{2.7}$$

(P_v) / (P_{in}) ratio : This parameter defines the ratio between the power transferred to the variator to the total incoming power into the transmission quantitatively. For fig(2.3), it is given as follows,

$$\frac{P_v}{P_{in}} = \frac{T_2 * \omega_2}{T_1 * \omega_1} \tag{2.8}$$

Using the aforementioned parameters, the given configuration of Toyota prius transmission architecture is investigated. The dependency of G_v and G_{eff}, as well as the dependency of variator power flow ratio ((P_v) / (P_{in})) on the G_{eff} were figured out and charted .

2.5 Prius Architecture Analysis

Through the application of equation (2.5) - equation (2.8), the given Prius architecture was analysed and the observations are mentioned as follows,

The dependency between G_v and G_{eff} is given by equation (2.9)

$$G_v = G * (1 - G_{eff}) + G_{eff} \tag{2.9}$$

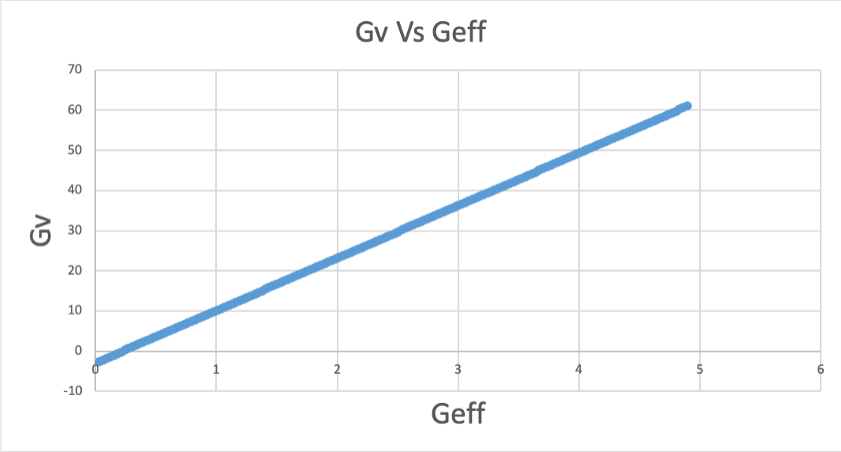

Figure 2.5: G_v vs G_{eff} for Prius Cruise Mode

It is observed that , with increase in G_{eff}, the G_v also increases. Electric motors have a maximum limit on the torque and the rpm (ex: 8810 rpm for Chevy Bolt motor). Thus at higher G_{eff}, the motor would not be able to provide the higher torques therefore limiting the ratio range.

Similarly,the dependency between $((P_v)$ / $(P_{in}))$ and G_{eff} is given by equation (2.10)

$$\frac{P_v}{P_{in}} = \frac{T_2 * \omega_2}{T_1 * \omega_1} = \frac{-1}{1 - G} * (1 - G + \frac{G}{G_{eff}}) \tag{2.10}$$

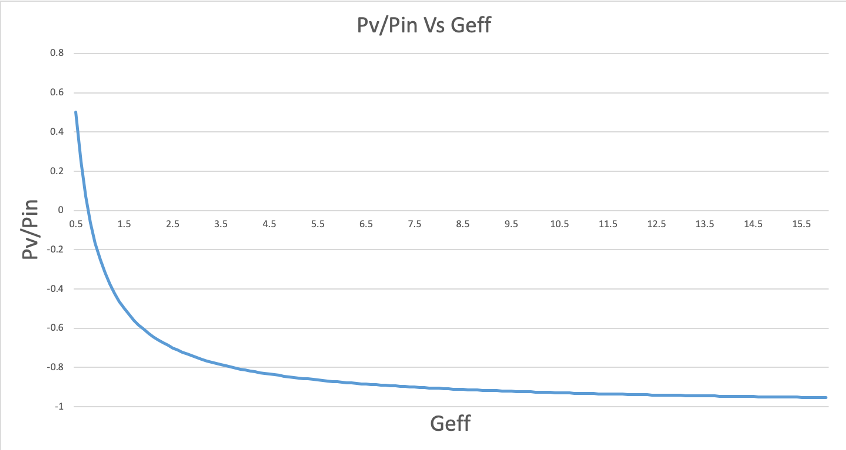

Figure 2.6: (P_v) / (P_{in}) vs G_{eff} for Prius Cruise Mode

In fig (2.6) it is observed that, at higher G_{eff} , the power transfer into the MGUs is pretty high. This would lead to higher losses as power transmission through the variator has lower efficiency. To circumvent this issue, manufacturers use clutches to allow themselves different modes to operate this architecture as previously mentioned in section (2.2)

All these observations are for the Basic ratio of -3.

2.6 Proposed Architecture and Analysis

Thus it is seen that to implement the power split architecture in EVs, changes are required to be made to the architecture to facilitate a wider ratio range for operation.

With a single power split, the overall control strategy gets restricted to manipulation of MGU1 motor speed which is connected directly to the PGT power split device. To facilitate more options in the control strategy, the addition of subsequent power splits into the given architecture is investigated. It is also possible that the power splitting device could consist of multiple PGTs to facilitate the split. Figure (2.7) shows the idea of the subsequent power split at source.

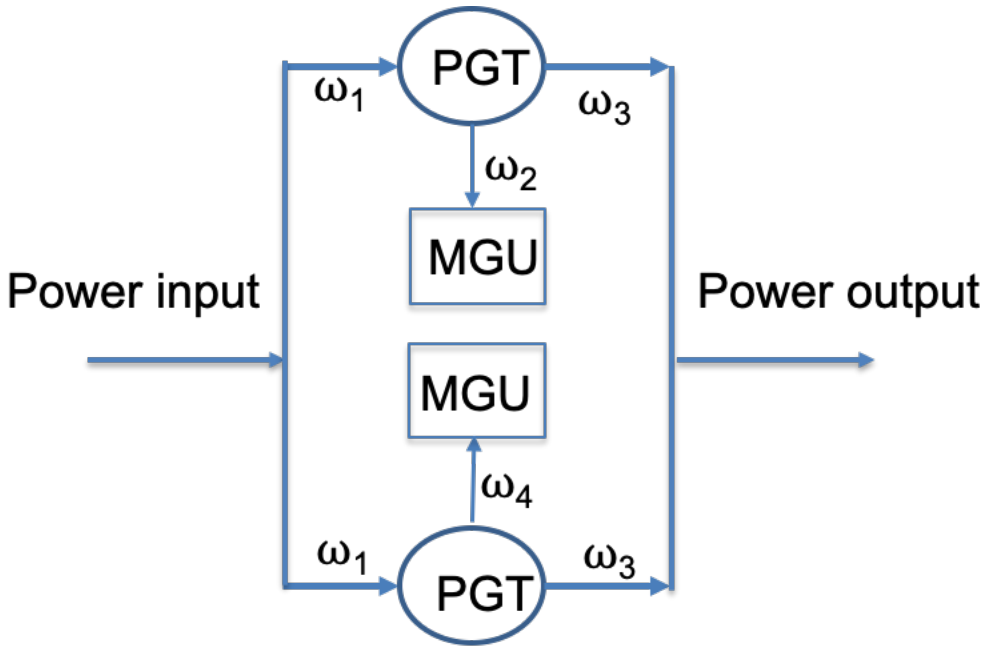

Figure 2.7: Dual Power Split Architecture

Thus, power is split initially at the source through the application of dog gears. The resulting two power branches are supplemented with a PGT each to channelize the power through their respective MGUs connected to them. Through this, it is intended to control the overall transmission ratio by individually controlling the torques and speeds of the motor generator units.

The G_{eff} formulation remains the same, the G_v formulation is given by the ratio between ω_2 and ω_4.

The dependency of G_v and G_{eff}, as well as the dependency of variator power flow ratio ((P_v) / (P_{in})) on the G_{eff} are given in equation (2.11) and (2.12) .

$$G_v = \frac{1 - G2'}{1 - G1'} * \frac{G_{eff} - G1'}{G_{eff} - G2'} \tag{2.11}$$

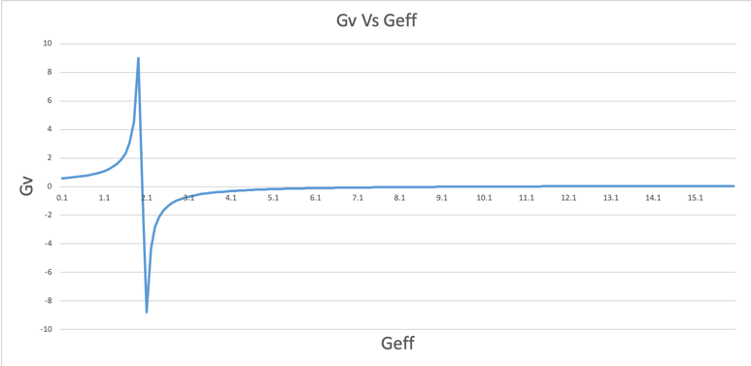

Figure 2.8: G_v vs G_{eff} for Dual Split Architecture.

It is observed that the G_v,vs G_{eff}, graph experiences a constant value behavior for a wider range of ratios than the Prius transmission. This allows for significant increase in motor operation ability while facilitating higher G_{eff}.

$$\frac{P_v}{P_{in}} = \frac{G_{eff} - G2'}{G1' - G2'} * (\frac{G1'}{Geff} - 1) \tag{2.12}$$

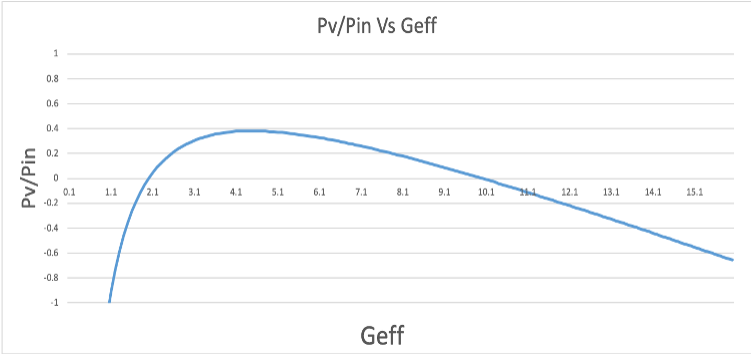

Figure 2.9: (P_v) / (P_{in}) vs G_{eff} for Dual Split Architecture .

Similarly it is seen for $((P_v)$ / $(P_{in}))$ that the graph demonstrates a quadratic behavior, and also establishes a low $((P_v)$ / $(P_{in}))$ ratio for a significantly wider range of effective transmission ratios.

It is noted that equations (2.11) and (2.12) are in the terms of the transmission ratios (G1' and G2') of PGT1 and PGT2 transmission sets respectively.

The derivations of equations (2.09),(2.10),(2.11),(2.12) can be found in appendix A1.1 and A1.2.

Thus it is observed that the dual split architecture does have the potential to operate the EV vehicles with higher G_{eff} with lower transmission of power into the variator. It consists of the prime motor as the primary power device with 2 other MGUs connected with the same battery. Through control strategies, the MGUs would be operated to facilitate an optimized G_{eff} and simultaneously deliver the expected power output at the vehicle.

The drawback to the given proposed architecture is the addition of weight and rotational inertia through the system which threatens to diminish the potential gain in the range. The architecture will be simulated against EPA drive schedules and the performance will be bench-marked against existing road vehicles for our benefit.

Fig (2.10) shows a functional representation of the proposed architecture.

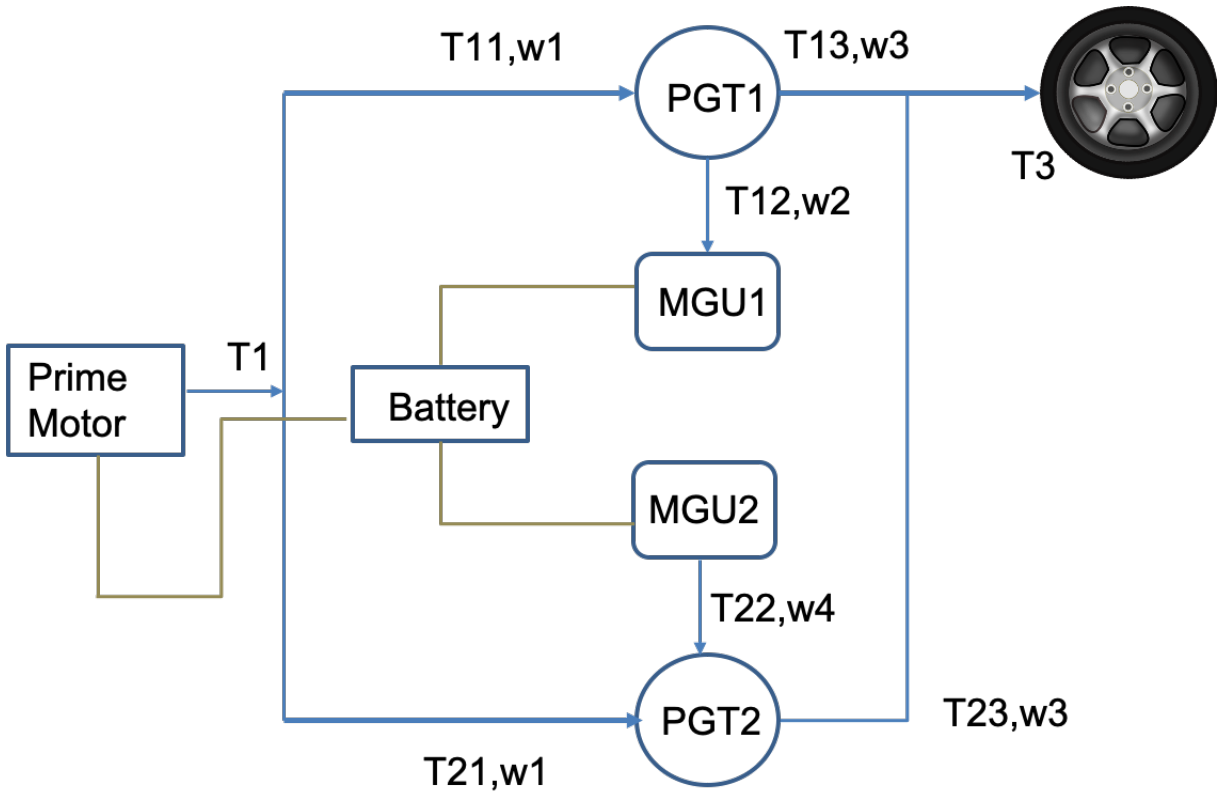

Figure 2.10: Proposed Dual Split Architecture.

In figure(2.10), T11,T12, T13 represent the torques in the input, controlled and output branches of the PGT1 gearset respectively. Similarly T21,T22, T23 represent the torques in the input, controlled and output branches of the PGT2 gearset respectively.

3. MODELLING OF BASE MODEL

Before proceeding to test the proposed architecture through simulation, A base model, comprising of a popular low weight passenger car complete with the requisite systems for range analysis, is modeled. This is primarily done to establish and evaluate modelling assumptions and also to have a benchmark against which the proposed architecture will be tested.

3.1 Chevy Bolt Parameters

The Chevy Bolt was designed by GM in 2016 to be its main offering in the Battery Electric Vehicles (BEV) section. The Bolt is powered by a 60 KW Hr Nickel rich Lithium Ion battery pack built by LG chem. The vehicle also uses a single reduction gear transmission architecture in a front wheel drive and such architectures are used in a majority of the low weight single drive passenger vehicles. The EPA estimated range of the vehicle is 238 miles over a combined highway and an urban driving cycle. It was also the second highest selling EV in US for 2017.

Thus the Chevy Bolt is chosen as the bench-marking model as it is popular and represents the single motor single gear transmission architecture appropriately. Table (3.1) shows some of the parameters of the Chevy Bolt that have been utilized in the model [17].

Specification	Value
Wheelbase	102.4 inches
Width	69.5 inches
Height	62.8 inches
Curb Weight	1616 Kg
Battery energy	60 KW Hr
Motor Peak Power	150 KW
Single Reduction Gear Ratio	7.05

Table 3.1: Specifications of the Chevy Bolt (2016) Model.

The various sub modules that have been implemented in this model are shown in fig (3.1).

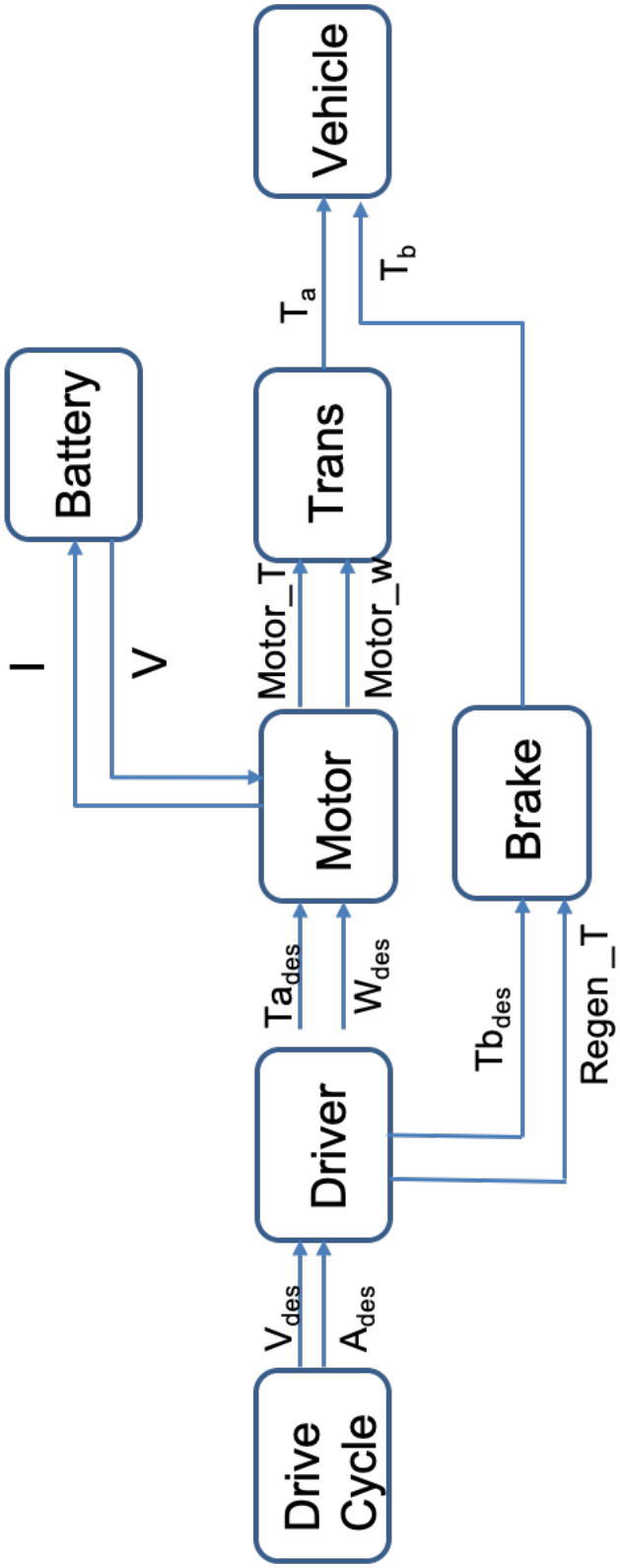

Figure 3.1: Schematic Representation of Base Model

The figure also shows the flowchart of control commands and power through these sub-modules. The model also implements some assumptions as mentioned below,

- Mechanical Transmission Efficiency is assumed to be 90 percent [18]. The efficiency of the mechanical transmission elements are assumed to be 95 percent. The base module contains a single reduction gearbox coupled with a differential. Thereby the total efficiency of the entire system is 90 percent (0.95 * 0.95 = 0.90).

- Ambient Temperature operation : For the system level analysis, the operation of the electrical instruments is assumed to be carried out at ambient temperature. This assumption inherently assumes that the battery management system is able to regulate the thermal parameters properly.

- Battery performance degeneration is ignored. Similar to mechanical systems that experience fatigue after multiple cycles of loading and unloading, similarly the battery parameters also show a devaluation upon multiple cycles of charging and discharging. This feature has been disregarded in this analysis as longer sustainability of battery performance is beyond the scope of this study.

3.2 Sub-Modules

3.2.1 Drive Cycle Schedules

This sub-module contains the information of EPA drive schedules used for highway (Highway Fuel Economy Test) and urban driving (Urban Dynamometer Driving Schedule)[19]. The model will be running on these drive schedules to provide a range estimate for the vehicle under consideration. Along with the HWFET and UDDS cycles, the IM 240 cycle is also chosen as it consists of both slow as well as high speed driving. Being a shorter cycle, it is used for sub-module performance verification.

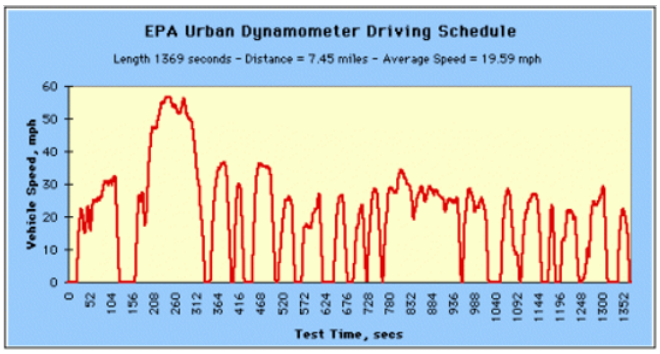

Figure 3.2: UDDS Drive Schedule

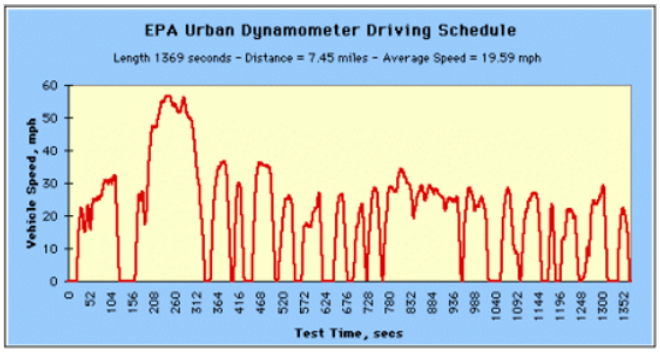

Figure 3.3: HWFET Drive Schedule

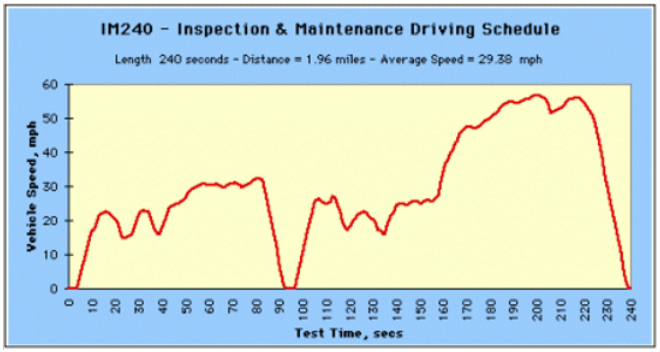

Figure 3.4: IM 240 Drive Schedule

The sub-module accepts the velocity as a time series data and outputs the desired velocity and the desired acceleration for the driver sub-module to function.

3.2.2 Driver

This sub-module basically replicates the functionality of a real time driver and tries to follow the drive schedule velocity as intended.The sub-module consists of two parts,

The physical section consists of a reverse vehicle dynamics function which takes in the desired velocity and the desired acceleration as inputs, and outputs the requisite torque and rotational speed of the prime motor. This is formulated as shown below,

$$T_{des} = (A_{des} * (M + \frac{I_w}{r^2}) + (C_0 + C_1 * V_{des} + C_2 * V_{des}^2)) * r \tag{3.1}$$

It also comprises of a control section which contains 2 sub parts- a PI control is implemented that acts upon the difference between the actual vehicle speed and the desired vehicle speed of the vehicle and a correction torque is added to the desired torque for better velocity following.

It also contains an implementation of a control strategy through which the maximum amount of regeneration torque possible from a given demand of braking torque at the given rotational speed is calculated. The algorithm for the regenerative torque division is discussed subsequently.

Regenerative Torque Division Algorithm: It is well known that motors can harvest kinetic energy and convert it into electrical energy under braking conditions for a vehicle. The motor becomes a generator and the harvested electrical energy is utilized for charging the battery. Regeneration strategy is very important in improving the range estimate for a vehicle as under complete friction braking, the kinetic energy would have been dissipated as unusable heat energy. Although during hard braking conditions, regenerative energy alone can not bring the vehicle to a complete stop. Thus both regeneration and friction braking are used in tandem in modern electric vehicles. The regenerative capacity is often limited by the motor operational limits and the instantaneous SOC (State of Charge) of the vehicle's battery.

State of charge (SOC) is the level of charge of an electric battery with respect to its capacity.

It is analogous to the fuel gauge in an IC engine powered vehicle. In this modelling exercise , we have introduced dependencies of the regenerative capacity on vehicle speed and instantaneous SOC.

In hybrid vehicles, it is observed that regeneration capacity diminishes at low speeds. This occurs as at low speeds, the available kinetic energy is pretty low. To harvest this kinetic energy into usable electric energy, the rectifier (converts A.C to D.C) needs to convert it at the DC bus voltage level (400V - 800V). Such conversion is inhibited at low vehicles thus at low speeds, vehicles exclusively use friction braking.

To model this at a system level, we inhibit the regeneration capacity to 0 percent at speeds below 5mph and gradually increase the capacity to 100 percent linearly at 15mph.

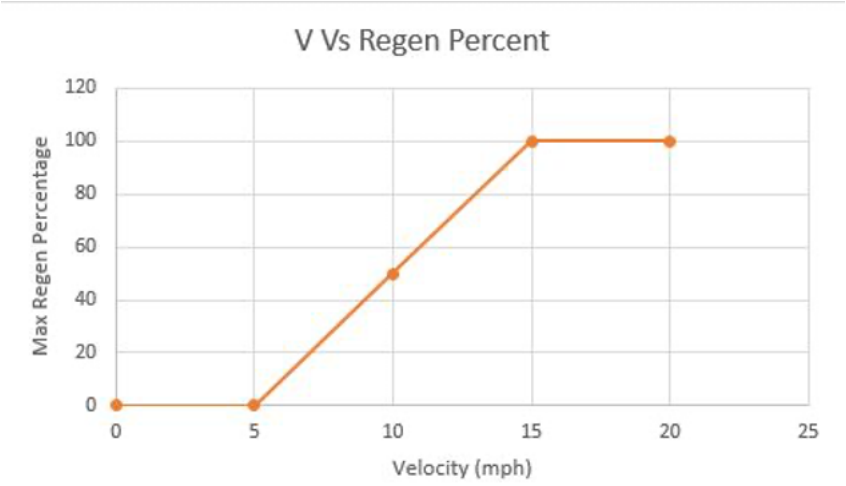

Figure 3.5: Regeneration Capacity Dependence on Vehicle Velocity

Similarly, when the SOC of the battery is near full capacity, the regeneration capacity is inhibited to not allow excessive electrical energy to enter the system. This is modelled as a linear depreciation from 100 percent regenerative capacity at 97 percent SOC to 0 percent regenerative capacity at 100 percent SOC.

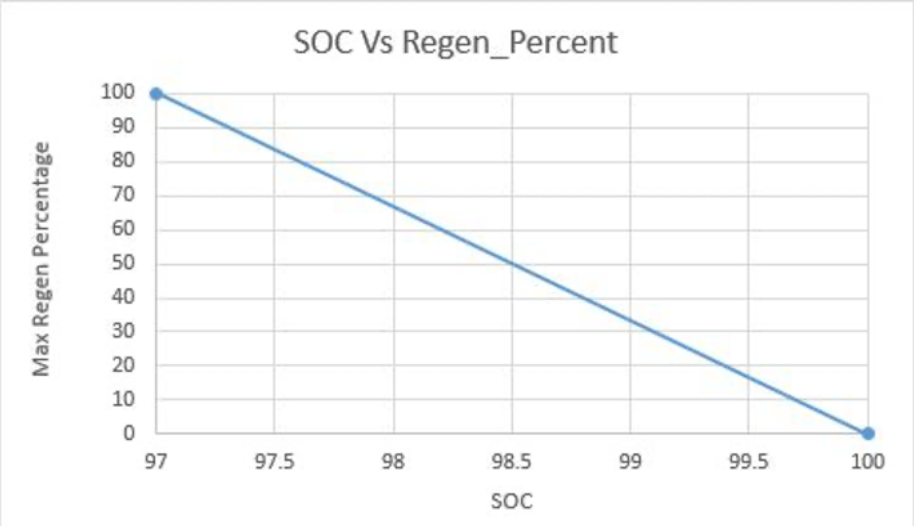

Figure 3.6: Regeneration Capacity Dependence on Battery SOC

Through these dependencies, the maximum regenerative torque that could be supplied to the motor is calculated. This maximum regenerative torque is then compared against the maximum torque capacity of the motor at the given speed. The algorithm is shown below.

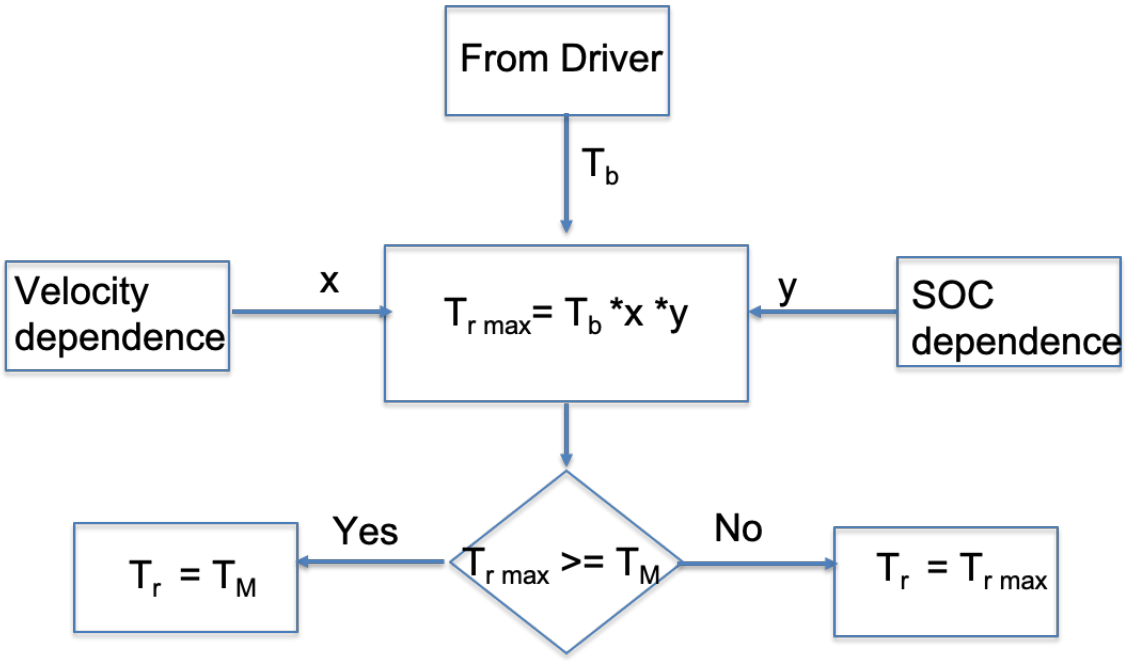

Figure 3.7: Regeneration Torque Division Algorithm

In fig (3.7) T_r, T_b, T_m, T_{rmax} represent the regeneration torque, desired braking torque, motor limiting torque at given motor speed and the maximum regenerative torque respectively.

Thus if the maximum regenerative torque, T_{rmax} is larger than the motor limiting torque (T_m), then T_{rmax} is the regeneration torque (T_r) . In the other case, the motor limiting torque (T_m) is the accepted as the motor regeneration torque.

3.2.3 Electrical Modelling

Battery

LG chem manufactures the Chevy Bolt battery which is a Nickel rich Lithium ion battery pack. It has the configuration of 96s 3p which refers to 96 cells connected in series and 3 cells connected in parallel. The battery pack also exhibits a rated charge capacity of 55 AH. To model this battery, the first order Thevenin circuit was adopted to develop the requisite equivalent circuit.

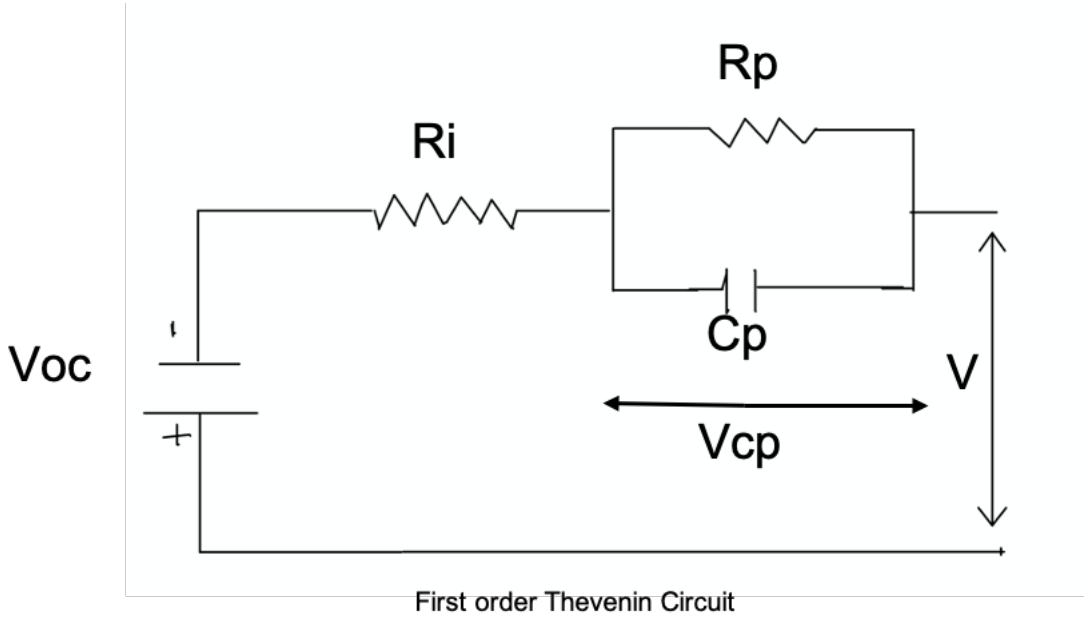

Figure 3.8: First Order Thevenin Circuit for Chevy Bolt Cell

The terminal voltage is calculated by using the formulae given below, which are estimated by

circuit element values dependent upon the instantaneous SOC (State of charge) of the battery[20,21].

The SOC is estimated through the coulomb counting method.

This model was selected to model the transient phenomena in Li-ion cells [22].

The following equations are used to calculate the battery voltage from the open circuit voltage (OCV).

$$V_{batt} = N_{batt_s} * (V_{oc} - I_{batt} * R_i - V_{cp} \tag{3.2}$$

$$SOC = SOCinit - \frac{\int_0^t I_{batt}\, dt}{3600 * C_b} \tag{3.3}$$

$$I_{batt} = \frac{I_{load}}{N_{batt_p}} \tag{3.4}$$

$$\frac{dV_{cp}}{dt} = \frac{-V_{cp}}{C_p * R_p} + \frac{I_{batt}}{C_p} \tag{3.5}$$

Each of these parameters are dependent on the instantaneous SOC and are modelled through look-up tables. The battery discharged an energy equivalent to 55 KWHr on a discharge current of 0.05C. The parameter SOC dependency graphs can be found in Appendix section(B.1)

Motor and Transmission

The Chevy Bolt motor is an 8 pole interior permanent magnet motor. It has a peak torque rating of 360 NM and a peak power rating of 150 KW. In our model, the motor efficiency map is used to replicate the motor operations [23].

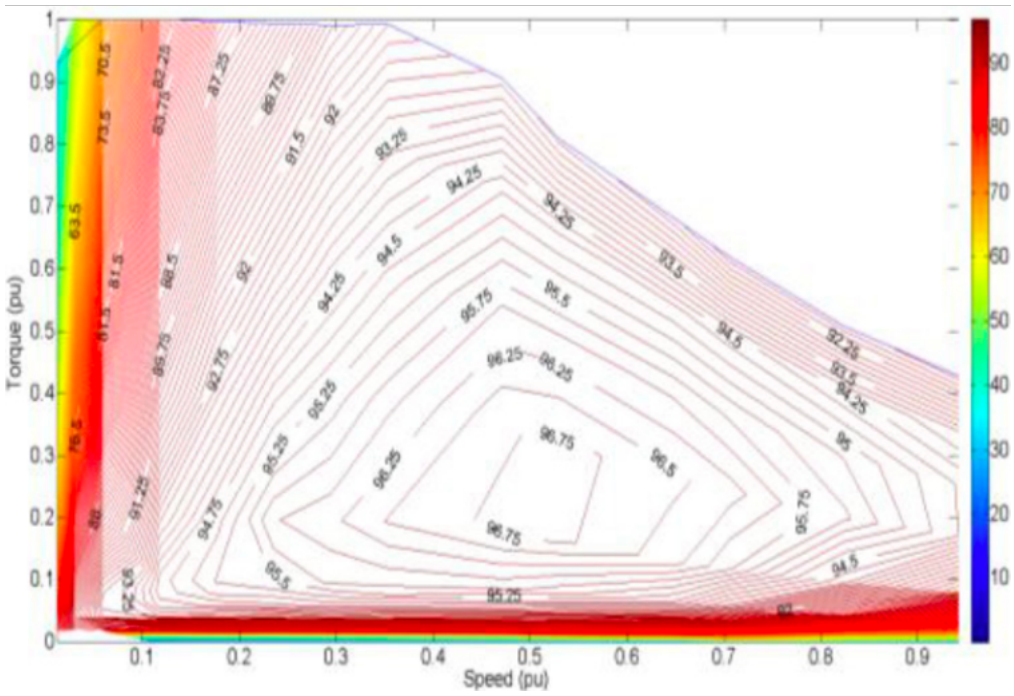

Figure 3.9: Chevy Bolt Motor Efficiency Map [23]. [a]

[a] Reprinted with permission from "Electric Motor Design of General Motors' Chevrolet Bolt Electric Vehicle" by Momen, Faizul Rahman, Khwaja Son, Yochan Savagian, Peter, 2016. SAE International Journal of Alternative Powertrains. 5. 10.4271/2016-01-1228, pg 286 -293, Copyright 2016 by SAE International.

The motor model contains a function that calculates the motor operating efficiency for a given operating torque and rotational speed. Through this efficiency, the battery power consumed by the motor is calculated and subsequently the load current for the battery is estimated.

During discharging:

$$Battery\ Power = Motor\ Power / Motor\ efficiency$$

During recharging:

$$Battery\ Power = Motor\ power * Motor\ efficiency$$

After the calculation of the battery power, the load current is figured out as shown

$$I_{load} = Battery\ Power/V_{batt} \tag{3.6}$$

The motor dynamics are considered through the reflection of motor inertia and is explained subsequently.

Fig (3.10) is considered to understand inertia reflection.

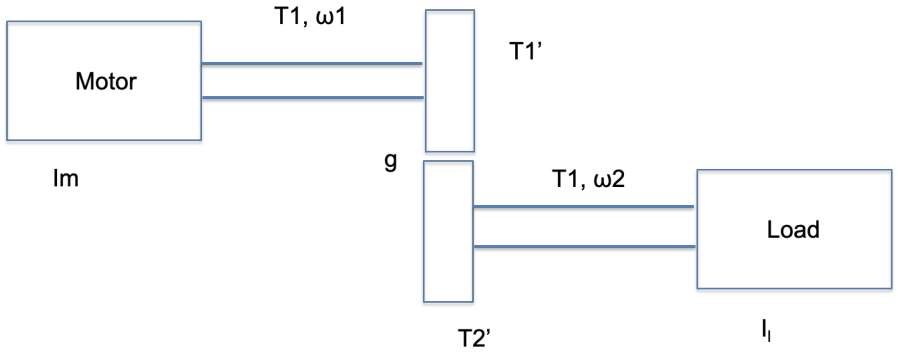

Figure 3.10: Reflection of Motor Inertia

In the above figure, the inertia of the gear system is ignored but the inertia of the motor (I_m) and load inertia (I_l) are considered. The gear ratio is referred to as 'g'. T1 and T2 represent the applied torques of the motor and the supplied torque at the load respectively.

Now,

$$T1' = T1 - I_m * \dot{\omega}1 \tag{3.7}$$

$$g = \frac{\omega 1}{\omega 2} = \frac{T2'}{T1'} \tag{3.8}$$

$$T2 = T2' - I_l * \dot{\omega}2 \tag{3.9}$$

Substituting equation (3.7) in (3.8) and using it in (3.9), we get,

$$g * T1 - ((g^2 * I_m) + I_l)\dot{\omega}2 = T2 \tag{3.10}$$

The single reduction gearbox gear ratio of Chevy Bolt transmission is 7.05.Thus using equation (3.10) this reflected inertia of the motor is added on the vehicle end for dynamic consistency.

3.2.4 Brakes

The brake Module is implemented to calculate the friction braking torque from a given desired braking torque. This formulation is shown in equation (3.11)

$$Friction\ braking\ torque = Desired\ braking\ torque - Regen\ braking\ torque. \tag{3.11}$$

3.2.5 Vehicle

This module contains functions that model the equations related to vehicle dynamics. Through this module , the vehicle's performance parameters such as acceleration and velocity is captured. The acceleration formulation is shown below.

$$a = \frac{(\frac{(T_a - T_b)}{r}) - (C_0 + C_1 * V_{act} + C2 * V_{act}^2)}{M + \frac{I_w + I_r}{r^2}} \tag{3.12}$$

3.2.6 Results and Verification

After completing the model, the model was simulated for all the drive cycles and the range was estimated. Important results are shown in the subsequent plots.

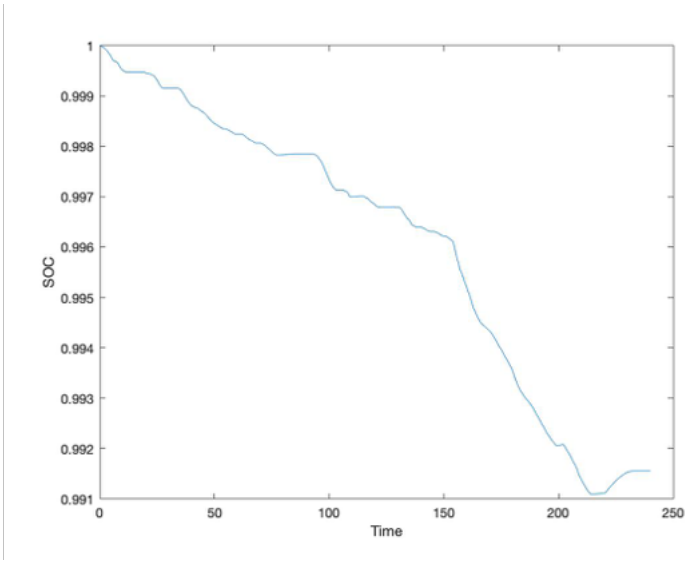

Figure 3.11: State of Charge Chart for IM 240 Cycle

The results of the IM 240 drive cycle are shown here. The SOC chart shows the drop of SOC for the full cycle. The rise in SOC during the braking phases is noticed due to the effect of regeneration.

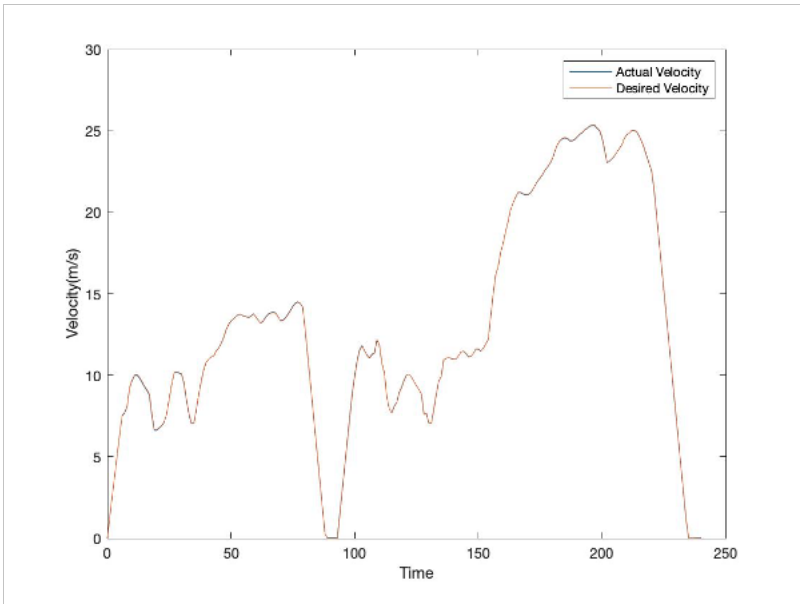

Figure 3.12: Velocity Comparison for IM 240 Cycle

Through the velocity comparison chart, it is also established that the the model follows the intended drive cycle accurately.

For verification with the Bolt model, the model's first order range estimation over a combined urban and highway driving cycle was calculated using the energy consumption as shown below. There is a charge correction factor multiplied with the total range which is considered due to the various charging options available for EV charging [24].

$$\begin{aligned} Range &= \frac{Miles\ travelled}{Battery\ Energy\ consumed} * total\ energy\ present * correction\ factor \\ &= \frac{(17.71) * 55 * 0.9)}{3.56} \\ &= 245.5\ miles \end{aligned}$$

The Chevy Bolt EPA rated range (2018) is 238 miles. Through this first order approach , the model functionality is verified.

In this section, the various control strategies and the requisite changes in dynamics associated with the new architecture are discussed.

The control strategies implemented in the model have two purposes. The first purpose is to generate an optimal overall transmission ratio that the system is required to be operated at in order to facilitate the higher efficiency of power transmission. Subsequently, the individual PGT + MGU strategies are also determined to satisfy the second purpose which is to facilitate the required G_{eff} and the requisite power at the vehicle. The inertia of the MGU units are reflected to the motor and to the vehicle accordingly and are discussed further in the dynamics subsection.

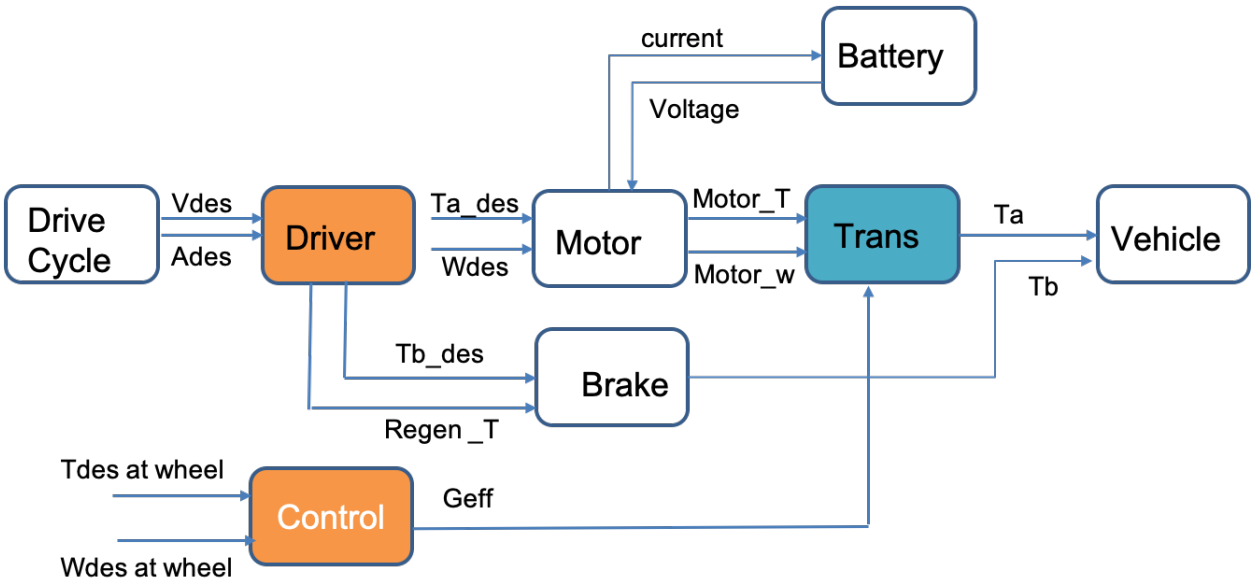

Figure 4.1: Schematic Representation of Proposed Architecture Model

The figure (4.1) displays a schematic representation of the model used for analysing the proposed architecture. The arrangement of sub-modules is similar to the base model although the sub-modules with changes in their functionality have been highlighted in the figure. The G_{eff}

generator is placed in the driver sub-module, whereas the individual control units for each of the PGT + MGU combination are placed in the transmission sub-module.

4.1 Dynamics

Consider the figure (4.2) where one possible single PGT configuration is showcased.

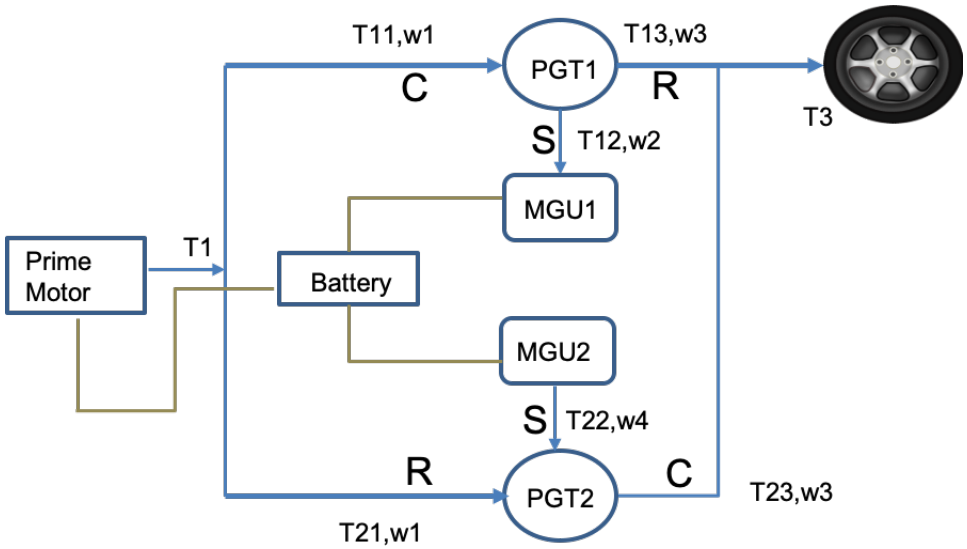

Figure 4.2: Proposed Architecture with a Single PGT Configuration

The PGT 1 has a configuration where the planetary carrier is the input gear, the sun gear is the controlled gear attached to the MGU and the ring gear is the output gear for this PGT - MGU combine. The notations T11, T12 and T13 represent the torques in the input , controlled and the output branches of the PGT respectively.

Similarly, the PGT 2 has a configuration where the ring gear is the input gear, the sun gear is the controlled gear attached to the MGU and the planetary carrier is the output gear for this PGT - MGU combine. The notations T21, T22 and T23 represent the torques in the input , controlled and the output branches of the PGT respectively.

w1 and w4 represent the rotational velocities of the MGU1 and MGU 2, whereas w1 and w3 represent the input and output speeds of the transmission architecture respectively.

As previously mentioned in sec (3.2.3) , the relationship between the applied torque and the transmitted torque is shown as follows

$$T_{applied} - I_m * \dot{\omega} = T_{transmitted}$$

This equation is applied to the prime motor and the two motor generator units.

Thus,

$$T1_{applied} - I_m * \dot{\omega}1 = T1_{transmitted}$$

$$T11_{applied} - I_m * \dot{\omega}2 = T11_{transmitted}$$

$$T21_{applied} - I_m * \dot{\omega}4 = T21_{transmitted} \tag{4.1}$$

The transmitted torque from prime motor is also expressed as

$$T1 = T11 + T21 \tag{4.2}$$

For a given torque from MGU 1 and MGU 2, using equation(2.5), T11 and T21 are represented as functions of the MGU torque and the basic ratio of the associated PGT.

$$T11 = f(T12, G1)$$

$$T21 = f(T22, G2) \tag{4.3}$$

Similarly w2 and w4 are represented in terms of w1 by using equation(2.4)and equation (4.2) is substituted in equation (4.1) and the following form of equation is obtained,

$$I_{mnet} * \dot{\omega}1 = T1' - T1.$$

Through the reflection of the MGU inertia for the motor, similar calculations were also undertaken for the vehicle end and the functional form of I_{mnet} and I_{vnet} for the shown configuration is as follows,

$$I_{mnet} = Im + Ic + Ir + (Im + Is) * ((G1 + 1) * (\frac{G1}{G_{eff}} - G1 + 1) + G2 * (G2 - (\frac{G2 - 1}{G_{eff}})$$

$$I_{vnet} = Iv + Ic + Ir + (Im + Is) * ((-G1 * (G1 - G_{eff} * G1 + G_{eff}) - (-G2 + 1) * (G2 * G_{eff} - G2 + 1)) \tag{4.4}$$

With these considerations, the MGU inertia is reflected on both the motor and vehicle end thereby effectively facilitating an inertia less consideration of the proposed transmission architecture for the implementation of the respective control strategies.

4.2 Geff Generator

The G_{eff} Generator is a sub module in the driver section. The purpose of this generator is to optimize the operating conditions for the prime motor at any given instantaneous power. The sub-module accepts the desired torques and rotational speed at wheel as its inputs. Through these parameters, the power required at the vehicle end is calculated. The relationship between Vehicle power and motor power is shown below,

For acceleration,

$$P_{motor} = \frac{Power\ at\ wheels/}{mechanical\ transmission\ efficiency}$$

for braking,

$$P_{motor} = (Power\ at\ wheels/) * (mechanical\ transmission\ efficiency) \tag{4.5}$$

The efficiency of the transmission is assumed to be 90 percent as mentioned in section (3.1). Through the above relationship, the Power required from the motor is calculated.

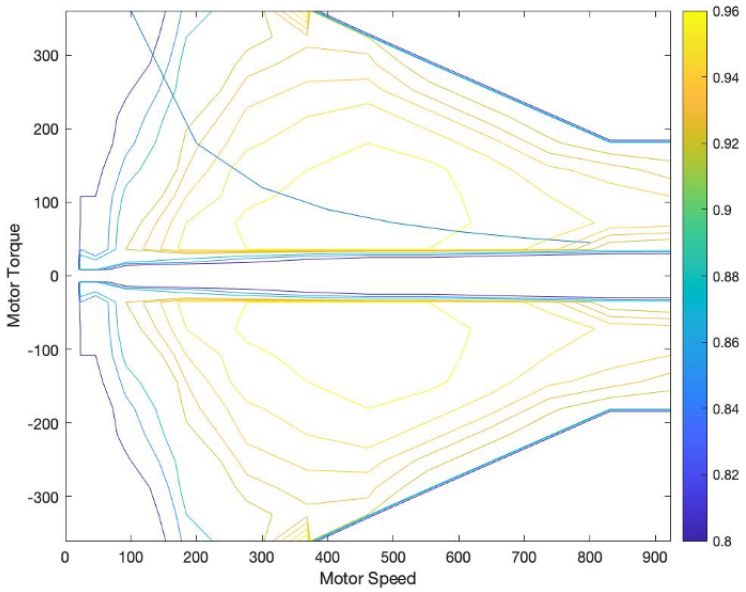

Figure 4.3: Motor Efficiency Map with Operation Points of Constant Power

The figure shown here shows the motor efficiency map of Chevy Bolt and the blue line represents a power of 100 KW. Now this power can be realized through various combinations of torque and rotational speeds facilitated through a change of gear ratios and formulated as shown below

$$T_m = \frac{Torque\ at\ wheel}{Gear ratio}$$

$$\omega_m = Rotational\ Velocity\ at\ wheel * Gear\ ratio \tag{4.6}$$

The operational efficiency for each gear ratio is subsequently evaluated and the gear ratio with the highest efficiency is selected to be the desired effective transmission ratio. This type of algorithm is known as a greedy algorithm as it optimizes the gear efficiency at any given instantaneous

demand of motor power.

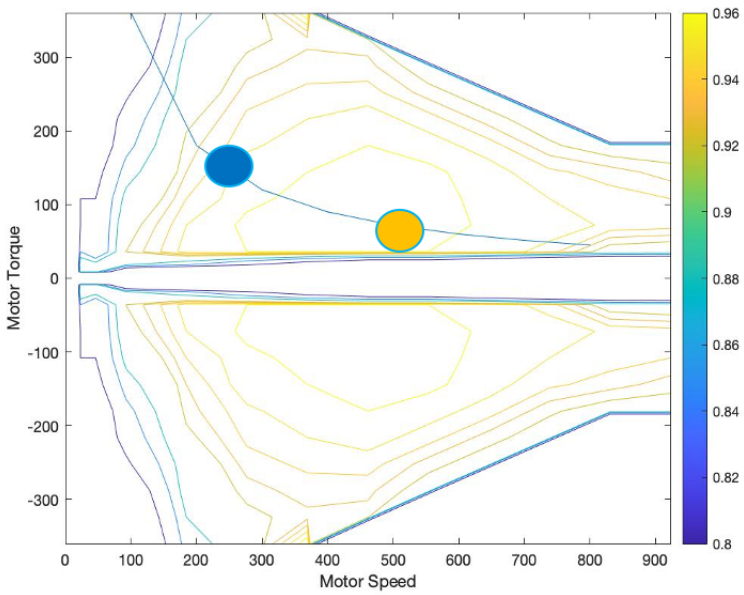

Figure 4.4: Effect of Changing Transmission Ratios on Motor Efficiency

Through the example shown in fig (4.4), it is observed that by choosing a lower gear ratio (yellow), a higher efficiency is achieved than previously achieved at the higher gear ratio (blue).

4.3 Transmission Control Strategy

To implement the desired G_{eff}, the 2 PGT + MGU combines are required to be controlled to operate at the designated points for the facilitation.

This is achieved by implementing closed loop speed control for PGT1 + MGU1. The main idea here is to reduce the error between the desired rotational speeds and the actual rotational speeds of the motors. Through reduction of error , the difference between the actual and desired G_{eff} is reduced and the requisite transmission ratio is achieved.

Feed forward torque control is applied on the other combine in order to maintain the power flow at the vehicle. The torque at MGU2 is decided through torque relationships between different

branches of PGT and is formulated as per the equation (2.5).

4.3.1 Closed Loop Velocity Control

In fig (4.2), as mentioned previously w1 and w3 represent the input and output speeds of the transmission. The desired values of w1 and w3 are determined through the G_{eff} calculator in the driver module and formulated as following

$$\omega 2_{des} = f(\omega 3_{des}, \omega 1_{des}, G) \tag{4.7}$$

Similarly, the actual values of w1 and w3 are determined through the inertia reflection calculations in the motor and vehicle modules.

$$\omega 2_{act} = f(\omega 3_{act}, \omega 1_{act}, G) \tag{4.8}$$

A PI control is implemented upon the error between the desired and the actual speed of the motor and the MGU 1 torque is determined.

$$T12 = PI * (\omega 2_{des} - \omega 2_{act}) \tag{4.9}$$

With the application of the equation (2.5) , the torques in the remaining branches of the PGT are figured out as functions of the motor torque and the basic ratio of the planetary gear train.

$$T11, T13 = f(T12, G1) \tag{4.10}$$

Thus through application of this control strategy, the torques and speeds of each of the branches of the planetary gear train is calculated.

4.3.2 Feed Forward Velocity Control

In fig(4.2), similar to the approach adopted in closed loop velocity control in MGU1, the actual rotational velocity of MGU2 is figured out as formulated below,

$$\omega 4_{act} = f(\omega 3_{act}, \omega 1_{act}, G2) \tag{4.11}$$

Now, the desired torque at the wheel is already known through the previously mentioned discussions in the driver sub-module for a given drive schedule. In knowledge of that information, T3 shown in fig(4.1) is known and is achieved through the summation of torques of T13 and T23 , the output branch torques for both the PGTs.

Since T13 is known through the velocity control implemented in PGT1 MGU1, The torque in the output branch of PGT2 is calculated according to the following formulation -

$$T23 = T3 - T13 \tag{4.12}$$

Similarly, Using equation (2.5), T22 and T21 are calculated accordingly

$$T22, T12 = f(T23 - T13) \tag{4.13}$$

With the application of the equation (4.13) , the torques in the remaining branches of the PGT are figured out as functions of the motor torque and the basic ratio of the planetary gear train. It is through these formulations, that the feed forward torque control is able to deliver the requisite power to the vehicle.

4.4 Results and Sanity Checks

Post the implementation of the control strategies of MGU motor control, The proposed architecture is tested against the drive schedules and some of the following results for the IM 240 drive schedule is shown here.

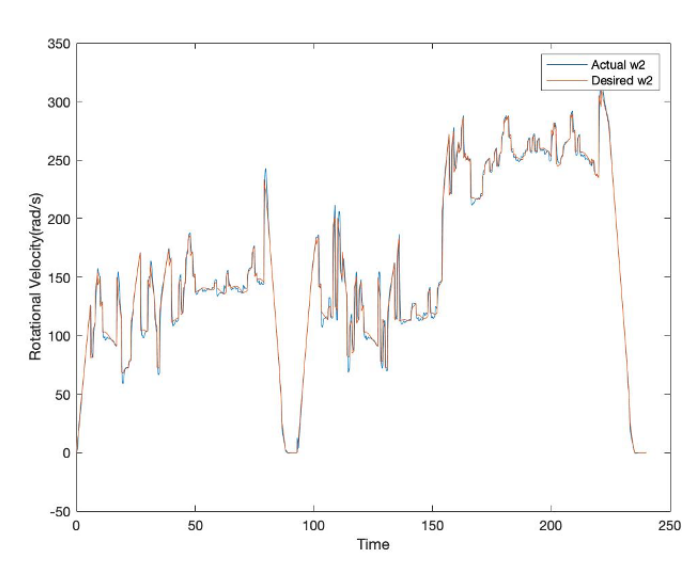

Figure 4.5: Velocity Control Performance of MGU1

Fig (4.5) shows that the velocity control on MGU1 performs well. There is minimal difference between the two velocities for the entire duration of the chosen drive schedule. This is an expected consequence of the implemented PI control.

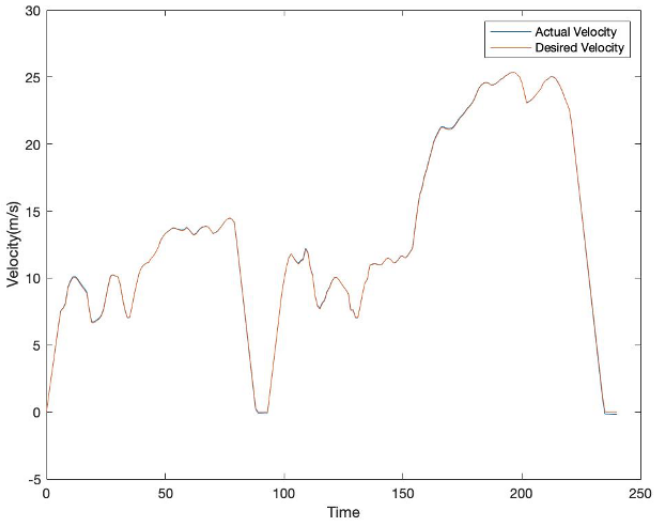

Figure 4.6: Desired and Actual Velocity Following of the Vehicle

Similarly, the effect of the successful implementation of both the control strategies can be shown through the close following established between the actual vehicle velocity and the desired vehicle velocity shown in fig(4.6). This acts as a verification for the feed forward torque control as the vehicles speeds are a direct function of the transmitted power at the vehicle end.

The conservation of power is shown in fig (4.7). The figure acts as a sanity check and establishes that the MGU-PGT combines do not produce any extra power. The power addition is given by

$$P_{PGT1} = T11 * \omega 1 + T12 * \omega 2 + T13 * \omega 3$$

$$P_{PGT2} = T21 * \omega 1 + T22 * \omega 4 + T23 * \omega 3 \tag{4.14}$$

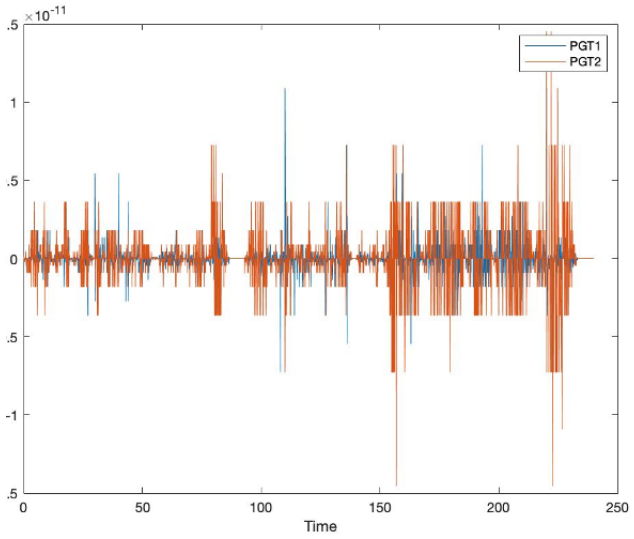

Figure 4.7: Conservation of Power in both PGTs

The power addition is in the order of 1e-12 as shown in the figure(4.7).

Finally, the following between the actual G_{eff} and the desired G_{eff} is shown in Fig (4.8).

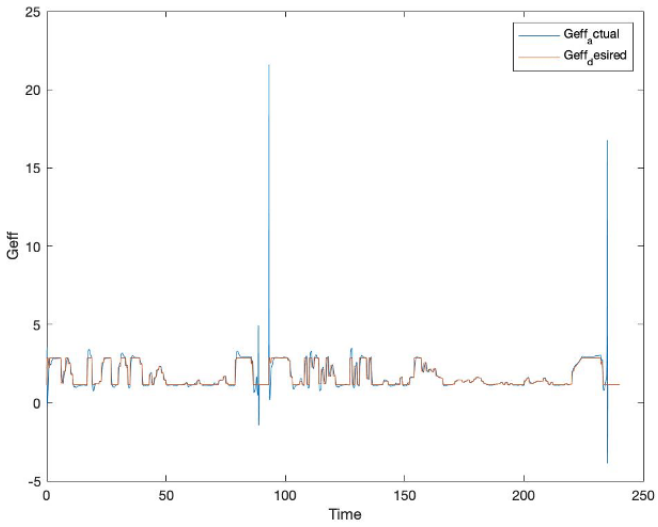

Figure 4.8: G_{eff}des and G_{eff}act Following Performance of the Architecture

This is shown to establish that all the associated parameters related to the functionality of the transmission architecture have performed along expected lines. The spikes noticed at the 100s and 230s mark are not representative of the system behavior. These spikes are seen during the braking phases of the vehicle and are simple the mathematical consequences of the way G_{eff} is calculated given by equation(2.6). At low speeds, both w1 and w3 approach zero and hence the actual w3 results in these spikes at those operational points.

In this section, the various possible configurations through which the configuration can be achieved is mentioned. As mentioned previously, there can be multiple configurations of planetary gear trains that can achieve the desired architecture. It is decided to study the single PGT configurations first and simulate them in order to achieve range extension. PGT configurations with multiple PGTs will be considered if the single PGTs fail to achieve any range extension across simulations. This is also done as multiple PGTs would not only increase the weight and cost but also increase the complexity of the entire system.

5.1 Configuration List

Assuming single PGT systems used in PGT1 and PGT2 in fig(4.2), the branches of each PGT has the nomenclature as shown in this diagram.

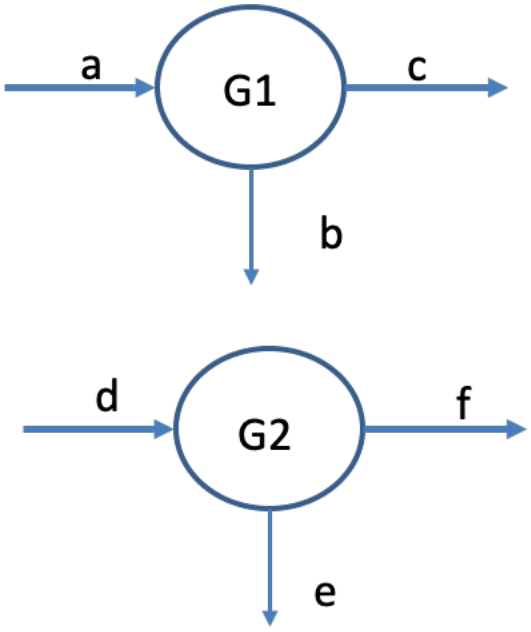

Figure 5.1: Nomenclature of Branches of PGT for Various Configurations.

Thus (a,b,c) refer to the input , motor-connected and output branches of PGT1 respectively. (d,e,f) refer to the input , motor-connected and output branches of PGT2 respectively.

The sun gear, planetary carrier and the ring gear may be arranged in 6 unique ways over a,b,c as shown here

Number	a	b	c
1	C	S	R
2	C	R	S
3	S	R	C
4	S	C	R
5	R	S	C
6	R	C	S

Table 5.1: Six Unique Configurations for a Single PGT.

Similarly, there exist the same 6 unique configurations for the branches of PGT2.

Thus therefore the total number of configurations that are unique for which the aforementioned architecture can be implemented is given in the Table(5.2)

Thus 36 different models are modelled according to the configurations presented in the table and are given identical configuration numbers as mentioned above. Subsequently each model has different dynamics and kinematics equations and are individually simulated to assess the effects of power flow caused by the change in arrangement of the PGT elements and are optimized accordingly to achieve the best range.

Number	a	b	c	d	e	f
1	C	S	R	C	S	R
2	C	S	R	C	R	S
3	C	S	R	S	R	C
4	C	S	R	S	C	R
5	C	S	R	R	S	C
6	C	S	R	R	C	S
7	C	R	S	C	S	R
8	C	R	S	C	R	S
9	C	R	S	S	R	C
10	C	R	S	S	C	R
11	C	R	S	R	S	C
12	C	R	S	R	C	S
13	S	R	C	C	S	R
14	S	R	C	C	R	S
15	S	R	C	S	R	C
16	S	R	C	S	C	R
17	S	R	C	R	S	C
18	S	R	C	R	C	S
19	S	C	R	C	S	R
20	S	C	R	C	R	S
21	S	C	R	S	R	C
22	S	C	R	S	C	R
23	S	C	R	R	S	C
24	S	C	R	R	C	S
25	R	S	C	C	S	R
26	R	S	C	C	R	S
27	R	S	C	S	R	C
28	R	S	C	S	C	R
29	R	S	C	R	S	C
30	R	S	C	R	C	S
31	R	C	S	C	S	R
32	R	C	S	C	R	S
33	R	C	S	S	R	C
34	R	C	S	S	C	R
35	R	C	S	R	S	C
36	R	C	S	R	C	S

Table 5.2: Thirty Six Unique Configurations for the Single PGT Implementation of the Architecture.

6. OPTIMIZATION

In this section, the optimization strategy for the chosen architecture is discussed. Given that there are many different configurations to implement the power split architecture, it is of paramount importance that the best configuration along with the best design variables is chosen to allow for higher range extension. The chosen algorithm for this exercise is described and the preceding and subsequent optimization analysis are also mentioned.

6.1 Design Space Exploration

Given the inter-dependency of various parameters and their consequential effects on the overall range of the vehicle, a design space exploration (DSE) is conducted to identify how the selected variables function over a given range of values. This helped in identifying the configurations that work and could result in a possible increase in range and also to understand how the design variables impact the overall operation of the architecture.

The DSE is made up of multiple factors (Design Variables) and levels (Value of Design Variables). For our model , the basic ratios of both the PGTs (G1 and G2) and the Differential gear ratio (FDR) are considered to be our factors with 3 levels of design values. The factors and the corresponding levels are shown in Table (6.1).

Experiment	G1	G2	FDR
1	-1.5	-1.5	2
2	-3	-3	2.5
3	-5	-5	2

Table 6.1: DSE Factors and Levels.

In the table below, the performance of each configuration for each of the aforementioned experiments for the IM 240 cycle is shown.

Configuration	Experiment 1	Experiment 2	Experiment 3
1	N	N	N
2	N	N	N
3	Y	N	N
4	Y	N	N
5	Y	N	N
6	Y	N	N
7	N	N	N
8	N	N	N
9	Y	Y	Y
10	Y	Y	Y
11	Y	Y	N
12	Y	N	N
13	N	N	N
14	N	N	N
15	N	N	N
16	Y	Y	Y
17	N	N	N
18	Y	Y	N
19	N	N	N
20	N	N	N
21	Y	Y	Y
22	N	N	N
23	Y	N	N
24	N	N	N
25	N	N	N
26	N	N	N
27	Y	N	N
28	Y	N	N
29	N	N	N
30	Y	N	N
31	N	N	N
32	N	N	N
33	Y	Y	Y
34	N	N	N
35	Y	Y	Y
36	N	N	N

Table 6.2: DSE Results for All Configurations .

The ‘ Y ‘ represents a comparable reading of the end of cycle SOC with that of the base Chevy Bolt model. The ‘N’ represents cases where the battery was completely discharged due to high re-circulation of power within the MGUs.

It is observed that in lower values of G1 and G2 , the configurations were also showing better results. No such assertions could be made for the FDR. These assertions are evaluated in the detailed intra-configuration optimization .

Thus, 19 configurations did not return a feasible SOC value. Out of the remaining configurations, configuration 21(SCR, SRC) and configuration 33 (RCS, SRC) returned the most promising results.

These configurations are further evaluated with optimization conducted on the values of the design variables.

6.2 Genetic Algorithm

Genetic Algorithm (GA) is a type of heuristic based algorithm that is operates upon the survival of the fittest concept for optimizing objective functions.

It generally consists of an initial population that represent the various set of values of design variables for which the objective function is going to be evaluated. The value of the objective function evaluated at the population values is known as the fitness function.

The individuals with the higher fitness values have higher probabilities of being chosen. Upon being chosen, their off springs (next generation of design variables) compete among each other. This process is continued till the fitness values converge and no more significant improvement in the fitness value is noticed.

There are also some hyper parameters that are associated with GA that affect the overall performance of the optimization. Some of the parameters are discussed here and are used in our optimization study.

Population size : This determines the total no of sets of design variables that are created at the initial generation for the optimization.

Elite Count : It is the minimum number of individuals that survive into the next generation

from the current generation.

Crossover function : This specifies a fraction of the population created by crossing over the design variables in each individual from the previous generation of the population and is decided by the crossover function.

Migration fraction : The fraction of population in each subset of a population that is mixed with other individuals in a different subset of the population.

Function Tolerance : The limiting value of the change in fitness function evaluation that terminates the optimization if the average change is less than it.

Parameter	Value
Population Size	30
Crossover Fraction	0.7
Function Tolerance	1e-19
Maximum Generations	30
Elite Count	5
Population Size	0.2

Table 6.3: Values of GA Hyper-parameters.

The upper and lower limit of the design variables is given as follows- G1[-1.5,-10], G2[-1.5,-10], FDR[2,3.5]

Thus the problem statement of the optimization exercise is to maximize the end of cycle SOC with constraints on maximum difference between the actual and desired speed profile of the vehicle to be less than 3mph.

6.3 Results

Through this approach, the configurations were evaluated and it was observed that configuration 21 (SCR,SRC) had the highest range estimate.

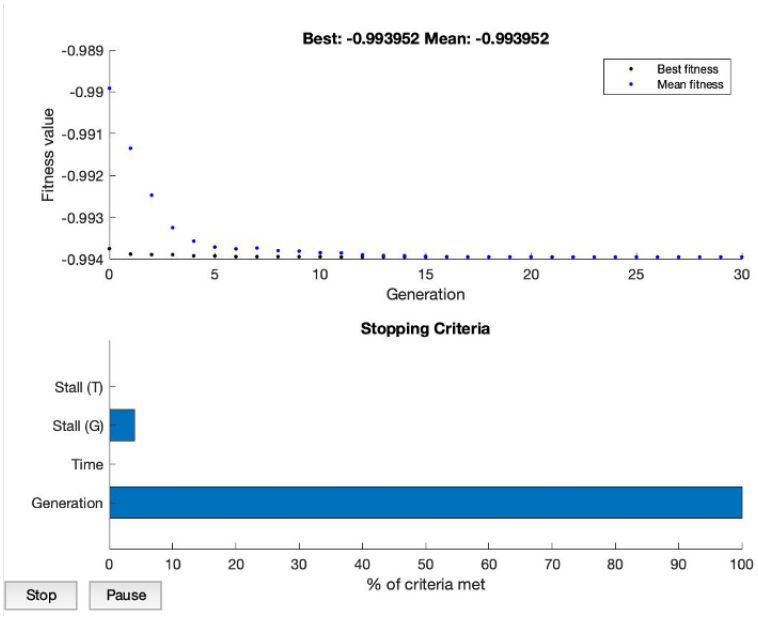

Figure 6.1: Optimization Results for Configuration 21

In fig(6.1) it is shown that the mean value as well as the best fitness value have converged after the end of 30 generations. The values of the optimized parameters are shown in Table (6.4).

Parameter	Value
G1	-1.506
G2	-1.506
FDR	3.4

Table 6.4: Value of Optimized Parameters.

The range estimation over the highway and the urban drive cycles with a supplemental addition of weight of 70 Kgs, due to the 2 extra MGUs and an extra PGT, is given as follows

$$
\begin{aligned}
Range &= \frac{Miles\ travelled}{Battery\ Energy\ consumed} * total\ energy\ present * correction\ factor \\
&= \frac{(17.71) * 55 * 0.9)}{3.14} \\
&= 279\ miles
\end{aligned}
$$

Thus there has been a 13.6 percent increase in the range from the base Bolt model.

6.4 Sensitivity Analysis

Although the simulated optimization does show a substantial increase in the range, the calculations are subject to the major assumptions that are intrinsic to the calculations. To measure the robustness of the result, it is important to measure the co-relation between these assumptions and their effect on the final result. This is done through conducting a sensitivity analysis on the major assumptions made in this modelling exercise and are mentioned below.

- Mechanical transmission efficiency of 90 percent.
- Mass of addition of 2 MGUs + PGT leads to an increase of 70 Kg.
- Electric efficiency loss caused due to assumption of ideal battery performance controlled through BMS (Battery Management System) = 0 percent.

Reasonable considerations are made regarding the uncertainties associated with these assumptions and are implemented in the model accordingly.

The weight addition through 2 MGUs + PGT combination is varied by 20 Kgs on both sides. The net change is directly changed in the Mass properties expressed in the vehicle dynamics equations.

The mechanical efficiency is change by 5 percent on both sides of the assumption and is implemented through changes reflected in torque calculations in transmission and control strategy equations.

The electrical power inter-transmission efficiency is depreciated by 5 percent and is effected by multiplying a factor to the inter power transmission between the battery and the motor.

Figure (6.2) and (6.3) show the response of the objective function to the changes in mass and mechanical efficiency.

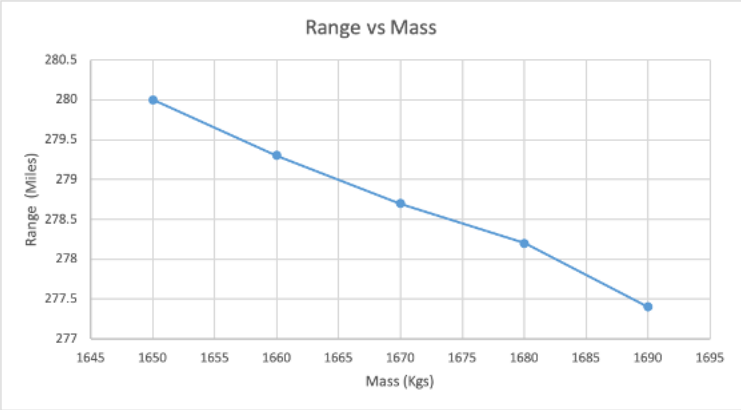

Figure 6.2: Variation of Range with Mass

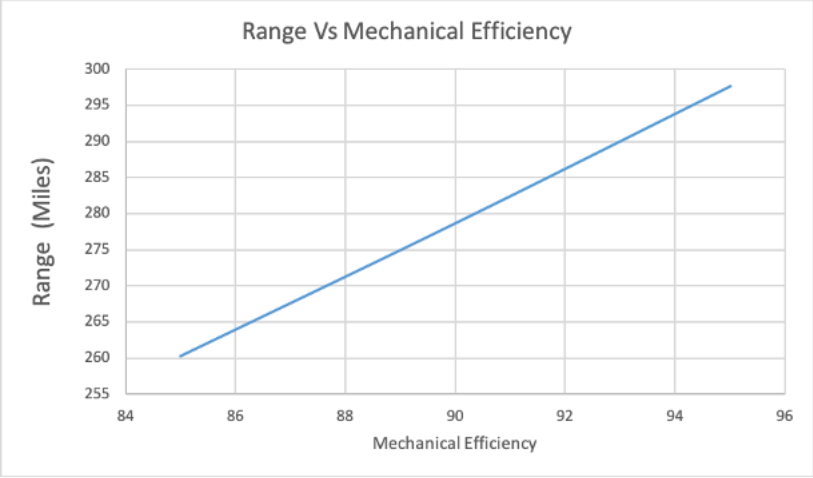

Figure 6.3: Variation of Range with Mechanical Efficiency

The depreciation of 5 percent in the electrical efficiency caused a drop of range by 9 percent.

Normalised Sensitivity shows the relative change, in percentage terms, of the fitness function for every unit percent change in the assumption. Normalised sensitivities of each of the three assumption parameter is calculated using the following equation,

$$Normalised\ Sensitivity = \frac{(\frac{\Delta J}{J})}{(\frac{\Delta X}{X})} \tag{6.1}$$

In equation (6.1), J and X represent the fitness function value and the value of the assumption at the optimized parameter respectively.

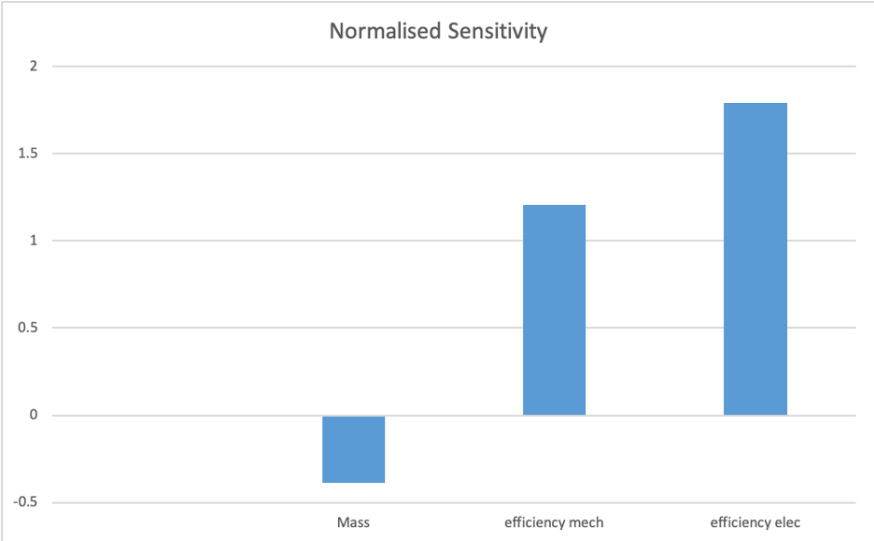

Figure 6.4: Tornado Chart Showing Normalised Sensitivity of the Assumptions

Through these calculations, the overall increase in the range was also recalculated to capture these effects. Table(6.5) shows the effect of the assumptions on the overall achieved range increase from the base model. The assumptions on mechanical and electrical efficiency are implemented for both the base and the proposed model, whereas the mass increase is only implemented in the proposed model.

Assumption	Range Increase (percent)
Mass increase by 20 kg	13.22
Mechanical efficiency of 0.85	11.24
Electrical efficiency of 0.95	9.94

Table 6.5: Change in Overall Range Gain Percentage with respect to the Change in Assumptions.

Thus it can be seen that electric efficiency and mechanical efficiency have a significant effect upon the range of the vehicle and thus need to be modeled at a higher fidelity in component level.

7. CONCLUSIONS AND FUTURE WORKS

7.1 Summary

To summarize, through this simulation, endeavors were made to analyze and identify architectures for potential increase in the nominal range of electric vehicles. Upon selection of the architecture, control strategies such as velocity and torque control were effectively applied in the proposed architecture to facilitate higher power conversion efficiency. Subsequently dual optimization at intra and inter configuration levels was conducted. Within configurations, the optimized effective transmission ratio required for the architecture to run the prime motor in the efficiency island were identified and at the inter configuration level, the best configuration and the requisite design variables for maximizing the range were found out.

Although the simulated optimization does show a substantial increase in the range, it is imperative to perform component level simulation through OEM data models with minimal assumptions to achieve higher fidelity and hence more robust results.

7.2 Future Works

- To create component level models for each module for higher fidelity and validation. System level modules do capture the basic functioning of the components, but nuances of the exact functionality can only be captured through component level modelling.

- To specify all the design parameters required for conversion of the architecture from CAD model to manufactured product. This would also require conducting strength analysis for all the components.

- To manufacture and test the proposed architecture to establish the viability and adaptability of such architectures in OEM vehicle platforms.

8. REFERENCES

1. Singh, K.V., Bansal, H.O., Singh, D. “A comprehensive review on hybrid electric vehicles: architectures and components.” J. Mod. Transport. 27, 77–107 (2019).

2. Mantriota, G. Case Study: “Infinitely variable transmissions with automatic regulation.” Proceedings of The Institution of Mechanical Engineers Part D-journal of Automobile Engineering - PROC INST MECH ENG D-J AUTO. 215. 1267-1280. 10.1243/0954407011528806 (2001).

3. Carbone, G., Mangialardi, L., Mantriota, G. “Fuel Consumption of a Mid Class Vehicle with Infinitely Variable Transmission.” SAE International Journal of Engines. 110. 2474-2483. 10.4271/2001-01-3692, (2001).

4. Bemporad A., Borodani P., Mannelli M. “Hybrid Control of an Automotive Robotized Gearbox for Reduction of Consumptions and Emissions.” In: Maler O., Pnueli A. (eds) Hybrid Systems: Computation and Control. HSCC (2003).

5. Zhu, W., Wang,X. “Design, Modeling, and Simulation of a Geared Infinitely Variable Transmission.” Journal of Mechanical Design. 136. 10.1115/1.4026950 (2014).

6. Cervantes-Culebro, H., Villar, C., Marrufo, O. “Infinitely variable transmission with orbital pulleys.” Advances in Mechanical Engineering. 11. 168781401988371. 10.1177/1687814019883717 (2019).

7. Miller, J. M. "Hybrid electric vehicle propulsion system architectures of the e-CVT type," in IEEE Transactions on Power Electronics, vol. 21, no. 3, pp. 756-767, May 2006.

8. Sheu, K.B. “Conceptual design of hybrid scooter transmissions with planetary gear-trains”. Appl. Energy 2007.

9. Zhang, X., Li, S., Peng, H., Sun, J. “Efficient Exhaustive Search of Power-Split Hybrid Powertrains with Multiple Planetary Gears and Clutches.” Journal of Dynamic Systems, Measurement, and Control. 137. 10.1115/1.4031533 (2015).

10. Ju, F. Zhuang, W , Wang, L. , Jiang, Yi. “A Novel Four-Wheel-Drive Hybrid Electric Sport Utility Vehicle with Double Planetary Gears”.IFAC-PapersOnLine. 51. 81-86. 10.1016/j.ifacol.2018.10.016 (2018).

11. Chung, C., Wu, C., Hung, Y. “Effects of Electric Circulation on the Energy Efficiency of the Power Split e-CVT Hybrid Systems.” Energies. 11. 2342. 10.3390/en11092342. (2018).

12. Chung, C.T.; Hung, Y.H. “Performance and energy management of a novel full hybrid electric powertrain system.” Energy 2015.

13. Bottiglione, F., De Pinto, S., Mantriota, G., Sorniotti, A. “Energy Consumption of a Battery Electric Vehicle with Infinitely Variable Transmission. “ Energies. 7. 8317-8337. (2014).

14. Ruan, J., Walker, P., Wu, J., Zhang, N., Zhang, B. “Development of continuously variable transmission and multi-speed dual-clutch transmission for pure electric vehicle.” Advances in Mechanical Engineering. 10. 168781401875822. 10.1177/1687814018758223. (2018).

15. Kim, D., Shin, K., Kim, Y., Cheon, J. “Integrated Design of In-Wheel Motor System on Rear Wheels for Small Electric Vehicle.” World Electric Vehicle Journal. 4. 597-602. 10.3390/wevj4030597. (2011).

16. Seyed Hosseini, Soheil. (2015). Case study: Toyota Hybrid Synergy Drive dr soheil seyed hosseini

17. "Chevy Bolt 2017" Accessed 10-7-2020.
<https://media.chevrolet.com/media/us/en/chevrolet/vehicles/bolt-ev/2017.tab1.html>

18. S. Derammelaere, S. Dereyne, P. Defreyne, E. Algoet, F. Verbelen and K. Stockman, "Energy efficiency measurement procedure for gearboxes in their entire operating range," 2014

IEEE Industry Application Society Annual Meeting, Vancouver, BC, 2014, pp. 1-9, doi: 10.1109/IAS.2014.6978376.

19. "Dynamometer Drive Schedules" Accessed on 10-7-2020. <https://www.epa.gov/vehicle-and-fuel-emissions-testing/dynamometer-drive-schedules vehicleDDS>

20. O. Hegazy, R. Barrero, J. Van Mierlo, P. Lataire, N. Omar and T. Coosemans, "An Advanced Power Electronics Interface for Electric Vehicles Applications," in IEEE Transactions on Power Electronics, vol. 28, no. 12, pp. 5508-5521, Dec. 2013.

21. Baccouche, Ines Jemmali, Sabeur Manai, Bilal Omar, Noshin and ESSOUKRI BEN AMARA, Najoua. (2017). Improved OCV model of a Li-ion NMC battery for online SOC estimation using the extended Kalman filter. Energies. 10. 764. 10.3390/en10060764.

22. Saldaña, G.; San Martín, J.I.; Zamora, I.; Asensio, F.J.; Oñederra, O. Analysis of the Current Electric Battery Models for Electric Vehicle Simulation. Energies 2019, 12, 2750.

23. Momen, Faizul Rahman, Khwaja Son, Yochan Savagian, Peter. (2016). Electric Motor Design of General Motors' Chevrolet Bolt Electric Vehicle. SAE International Journal of Alternative Powertrains. 5. 10.4271/2016-01-1228.

24. "Decoding Electric Car MPG" Accessed on 10-07-2020. <https://www.edmunds.com/fuel-economy/decoding-electric-car-mpg.html>

APPENDIX A

DERIVATION OF EQUATIONS

A.1 Effective Transmission Ratio and Variator Power Ratio

A.1.1 Prius Architecture

For the given configuration of prius where, $\omega 1$, $\omega 2$, $\omega 3$ refer to ωc, ωs, ωr respectively

$$G = \frac{\omega 2 - \omega 1}{\omega 3 - \omega 1} \tag{A.1}$$

Through the definition of G_v and G_{eff} , the above equation is expressed as

$$G = \frac{G_v - G_{eff}}{1 - G_e ff}$$

upon rearranging,

$$G_v = G(1 - G_{eff}) + G_{eff}$$

Similarly, to determine equation (2.10),

$$\frac{T2}{T1} = \frac{1}{G - 1}$$

and from equation (A.1)

$$\frac{\omega 2}{\omega 1} = 1 + \frac{G}{G_{eff}} - G$$

Thus,

$$\frac{P_v}{P_{in}} = \frac{T_2 * \omega_2}{T_1 * \omega_1} = \frac{-1}{1 - G} * (1 - G + \frac{G}{G_{eff}}) \tag{A.2}$$

A.1.2 Proposed Architecture

Using the definition of Transmission ratio G',

$$G1' = \frac{\omega 1 - \omega 2}{\omega 3 - \omega 2} \tag{A.3}$$

$$G2' = \frac{\omega 1 - \omega 4}{\omega 3 - \omega 4} \tag{A.4}$$

Now G_v = $\frac{\omega 2}{\omega 4}$

Rearranging equation (A.3) and (A.4), we get

$$G_v = \frac{\omega 2}{\omega 4} = \frac{1 - G2'}{1 - G1'} * \frac{G_{eff} - G1'}{G_{eff} - G2'} \tag{A.5}$$

Similarly,

$$\frac{\omega 2}{\omega 1} = \frac{(1 - \frac{G1'}{G_{eff}})}{1 - G1'}$$

$$\frac{T2}{T1} = G1' - 1$$

Now in fig (2.10), assume T1 = T, T11 = xT, T21 = (1-x)T, where x is the split fraction,

Applying eqn(2.5) with the definition of G',

$$x = \frac{G_{eff} - G2'}{G1' - G2'}$$

Thus,

$$\frac{P_v}{P_{in}} = \frac{G_{eff} - G2'}{G1' - G2'} * (\frac{G1'}{Geff} - 1) \tag{A.6}$$

A.2 Simulation parameters

Parameter	Value
M	1600 Kg
C0	0.0041 N
C1	6.6e-5 N/(m/s)
C2	0.5116 N/(m/s2)
I_m	0.2 Kg m2
I_w	0.4536 Kg m2

Table A.1: Values of Simulation Parameters.

APPENDIX B

SUPPLEMENTARY SIMULATION DATA

B.1 Look up Tables

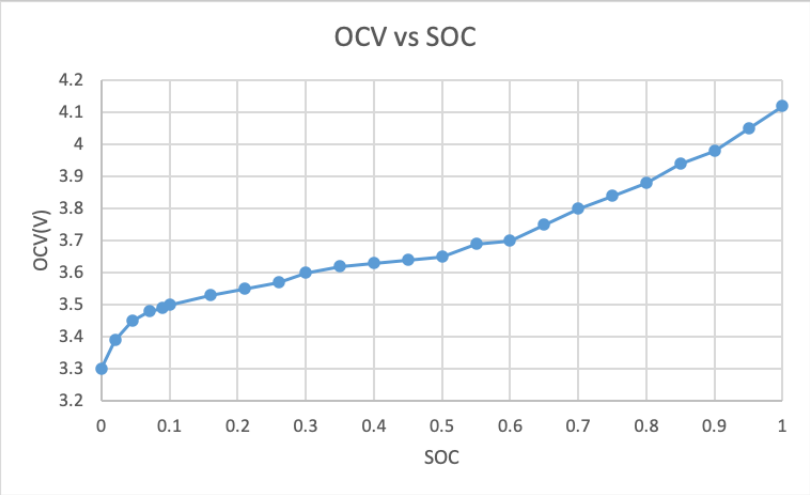

Figure B.1: OCV vs SOC Chart [21].

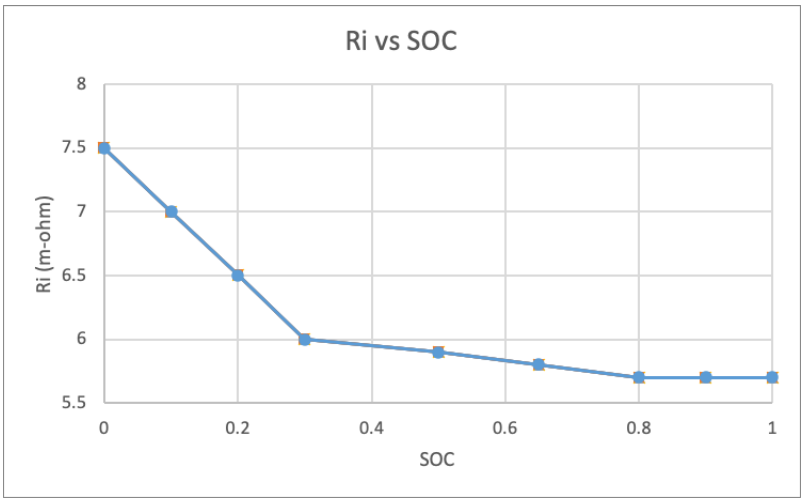

Figure B.2: R_i vs SOC Chart [20]. [a]

[a]Reprinted with permission from "An Advanced Power Electronics Interface for Electric Vehicles Applications" by O. Hegazy, R. Barrero, J. Van Mierlo, P. Lataire, N. Omar and T. Coosemans, 2013 in in IEEE Transactions on Power Electronics, vol. 28, no. 12, pp. 5508-5521, Copyright 2013 by IEEE.

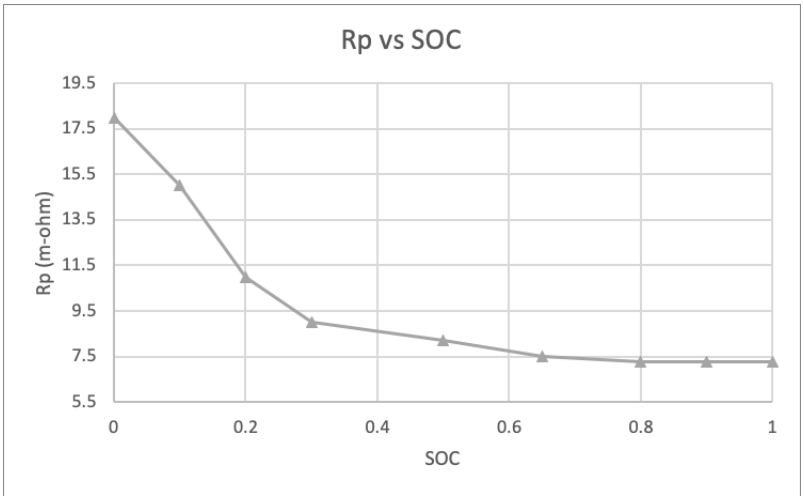

Figure B.3: $R_p$vs SOC Chart [20]. [a]

[a]Reprinted with permission from "An Advanced Power Electronics Interface for Electric Vehicles Applications" by O. Hegazy, R. Barrero, J. Van Mierlo, P. Lataire, N. Omar and T. Coosemans, 2013 in in IEEE Transactions on Power Electronics, vol. 28, no. 12, pp. 5508-5521, Copyright 2013 by IEEE.

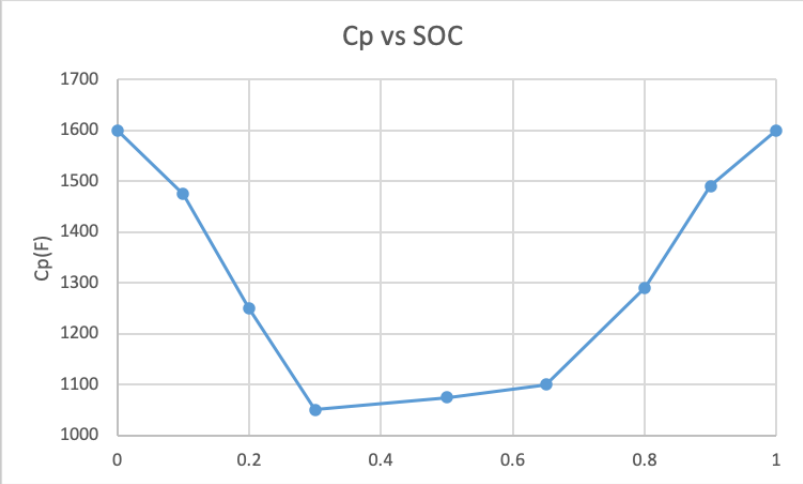

Figure B.4: C_p vs SOC Chart [20]. [a]

[a]Reprinted with permission from "An Advanced Power Electronics Interface for Electric Vehicles Applications" by O. Hegazy, R. Barrero, J. Van Mierlo, P. Lataire, N. Omar and T. Coosemans, 2013 in in IEEE Transactions on Power Electronics, vol. 28, no. 12, pp. 5508-5521, Copyright 2013 by IEEE.